Biophysical Journal
Article

Biophysical Society

Measuring Intracellular Viscosity in Conditions of Hypergravity

Emma M. Woodcock,[1,2] Paul Girvan,[1,2] Julia Eckert,[3,4] Ismael Lopez-Duarte,[1] Markéta Kubánková,[1] Jack J. W. A. van Loon,[4,5] Nicholas J. Brooks,[1,2,*] and Marina K. Kuimova[1,2,*]

[1]Department of Chemistry, Molecular Sciences Research Hub, Imperial College London, London, United Kingdom; [2]Institute of Chemical Biology, Imperial College London, South Kensington, London, United Kingdom; [3]Department of Physics, School of Science, Technische Universität Dresden, Dresden, Germany; [4]European Space Agency Technology Centre, TEC-MMG LIS Lab, Noordwijk, the Netherlands; and [5]Department of Oral and Maxillofacial Surgery/Oral Pathology, Dutch Experiment Support Centre, Academic Centre for Dentistry Amsterdam, VU University Medical Centre, Amsterdam, the Netherlands

ABSTRACT Gravity-sensitive cellular responses are regularly observed in both specialized and nonspecialized cells. One potential mechanism for this sensitivity is a changing viscosity of the intracellular organelles. Here, we report a novel, to our knowledge, viscosity-sensitive molecular rotor based on mesosubstituted boron-dipyrrin used to investigate the response of viscosity of cellular membranes to hypergravity conditions created at the large diameter centrifuge at the European Space Agency Technology Centre. Mouse osteoblastic (MC3T3-E1) and endothelial (human umbilical vein endothelial cell) cell lines were tested, and an increase in viscosity was found with increasing hypergravity loading. This response is thought to be primarily biologically driven, with the potential for a small, instantaneous physical mechanism also contributing to the observed effect. This work provides the first, to our knowledge, quantitative data for cellular viscosity changes under hypergravity, up to 15 $\times$ *g*.

INTRODUCTION

Gravity sensing in mammalian cells is a puzzling phenomenon (1–4). The small size of a single cell implies that a change in the gravitation environment would be unable to provide a change in force that could elicit a cellular response; however, initial evidence has been presented showing single cells responding to changes in gravity. For example, under microgravity, changes in the mammalian cell cytoskeleton (5) and in plant cell proliferation rates (6) have been observed. Moreover, both mammalian epithelial cells and plant cell walls have been reported to exhibit a mechanobiological response to hypergravity, compensating for the increased gravitational load (7,8). Although it is becoming clear that mammalian cells can respond to altered gravity, much is still unknown about the response pathways activated by changing gravity or about the variations in said pathways between cell types.

One potential mechanism for a cell to exhibit a mechanosensitive response is a change in viscosity of either the cell membrane and/or the intracellular organelles (9). Viscosity is a key regulator of diffusion-controlled reactions that influences reaction rates throughout the cell (10) and hence cellular signaling (11). Cellular viscosity has also been shown to be relevant to many diseases; abnormalities in red blood cell viscosity have been observed in sickle cell anemia (12) and type II diabetes (13,14), whereas changes in the mitochondrial membrane viscosity have been reported in numerous neurodegenerative diseases (15–17). The ability to investigate cellular viscosity changes under unusual gravity conditions may lead to advances in understanding the function of mechanobiological parameters in such diseases.

Advancements in fluorescence techniques have enabled a means for monitoring diffusion and kinetics in cells (18) and for exploring the structure and organization of cellular membranes (19). Molecular rotors, small synthetic fluorophores that change their fluorescence response depending on the environmental viscosity, recently allowed measurements of real-time viscosity changes on a single cell level in vitro and in vivo (20,21). In molecular rotors, fluorescence quantum yield and excited state lifetime respond strongly to the viscosity of the surrounding environment because of a marked viscosity effect on the nonradiative decay of their excited state via alteration of intramolecular rotation rates in a viscous environment. Hence, a change

Submitted November 12, 2018, and accepted for publication March 19, 2019.

*Correspondence: n.brooks@imperial.ac.uk or m.kuimova@imperial.ac.uk

Emma M. Woodcock and Paul Girvan contributed equally to this work.

Editor: Jochen Mueller.

https://doi.org/10.1016/j.bpj.2019.03.038

in the ratio between nonradiative and radiative excited state decay results in a sensitivity of molecular rotors to their immediate viscosity (22) and can be utilized in measuring viscosity of small cellular compartments, such as membranes (23) and organelles (24).

Here, we report the use of a molecular rotor to measure changes in viscosity of cellular membranes under altered gravity. To generate conditions of hypergravity, we utilized the large diameter centrifuge (LDC) facility, housed at the European Space Research and Technology Centre. Because creating hypergravity conditions requires highly specialist equipment, it is often not viable to measure diffusion events in this environment. However, because molecular rotors only require measurement of the fluorescence intensity, by placing a fluorescence microscope in the LDC, it is possible to directly image cells during exposure to an increased gravitational field, enabling us to visualize real-time changes in cellular viscosity.

For model systems, we first employed mouse preosteoblast cells (MC3T3-E1), a cell line commonly used in studies interested in cell mechanosensing of force and strain, as well as gravisensing research (25). We further expanded to human umbilical vein endothelial cells (HUVECs) because of their adaptability to a changing environment in vivo (26) like hypergravity and the impact of HUVEC viscosity on disease (12). This work delivers the first, to our knowledge, quantitative study of varying viscosity under conditions of hypergravity and, as such, aids the understanding of cell adaptation to abnormal environments. Furthermore, it provides an insight into cell rheology and responses to shear stress, such as blood flow, and will enable further investigation into lipid membrane compositions under anisotropic conditions, laying the foundation for additional mechanobiological research under altered gravity conditions.

METHODS

Absorption and fluorescence emission measurements

Fluorescence spectra were measured using a FluoroMax4 spectrofluorometer (Horiba Scientific, Northampton, United Kingdom) with a Xenon lamp excitation source. Spectra were corrected for wavelength-dependent efficiency of the light source and sensitivity of the detector. Quartz cuvettes with 1 cm pathlength were used in all measurements. For the response measurement of rotor 2 fluorescence (henceforth referred to as "2") to viscosity, fluorescence emission spectra were collected in 0–100% v/v methanol/glycerol mixtures of viscosities ranging between 0.6 and 1457.6 cP at 20°C. A 0.5 mM stock solution of 2 in dimethyl sulfoxide was used to make up the final solutions containing 1 μM of 2. Fluorescence was excited at 450 nm and collected between 465 and 700 nm.

Determination of quantum yield

The quantum yield of 2 was measured using fluorescein as a standard. The absorbance values were kept well below 0.1 to minimize inner filter effects. Integrated emission intensity (excited at 465 nm, collected between 480 and 700 nm) of 0.083–1 μM fluorescein in 0.1 M NaOH was plotted against absorbance values at 465 nm; a linear fit was used to obtain the gradient. Similarly, 0.25–2 μM of 2 in a 70:30 v/v mixture of glycerol/methanol was prepared, and integrated emission intensity (excited at 465 nm, collected between 480 and 700 nm) was plotted against absorbance at 465 nm; a linear fit was used to obtain the gradient for determining quantum yield according to the following equation:

$$\Phi_X = \Phi_{ST}\left(\frac{Grad_X}{Grad_{ST}}\right)\left(\frac{\eta_X^2}{\eta_{ST}^2}\right)$$

where $Grad_x$ and $Grad_{st}$ are gradients of the emission versus absorbance plots of the sample and fluorescein standard, respectively, and η^2_X and η^2_{ST} is the refractive index of the solvent for the sample and fluorescein standard, respectively. A quantum yield φ_{ST} of 0.79 was used for fluorescein in 0.1 M NaOH (27). The refractive indices of the 70:30 v/v mixture of glycerol/methanol (1.41 at 25°C) and fluorescein in 0.1 M NaOH (1.33) were obtained from literature (28).

Cell culture

MC3T3-E1 cells were obtained as a gift from Mr. Cor Semeins (Oral Cell Biology; Academic Centre for Dentistry Amsterdam, Amsterdam, the Netherlands). MC3T3-E1 cells were cultured in Minimum Essential Medium α (without ascorbic acid) (ThermoFisher Scientific, Carlsbad, CA) supplemented with 10% fetal bovine serum (ThermoFisher Scientific). HUVEC and the culture medium were obtained as a gift from Dr. Robert Szulcek (Vrije Universiteit Medical Centre, Amsterdam, the Netherlands). HUVECs were cultured in endothelial cell medium (ScienCell, Carlsbad CA), which contained 5% fetal bovine serum, 1% penicillin/streptomycin solution, and 1% endothelial growth cell supplement. Culture flasks and slides to be used with HUVECs were first treated with a 0.1% gelatin solution before cells were seeded. Cells were passaged when 70–90% confluent in 25-cm^3 flasks grown at 37°C and 5% CO_2. For imaging, cells were seeded onto eight-well cover glass chambers (Nunc Lab-Tek, ThermoFisher Scientific) at a density of 10^4 cell/well in 0.4 mL of culture medium and grown for 24 h to confluence. Before hypergravity exposure, the media was removed and replaced with media containing 5 μM rotor 2. The cells were left in the incubator for 30 min to allow the dye to be taken up by the cells. The media was removed, and the cells were washed twice in Hank's Balanced Salt Solution (no calcium, no magnesium; ThermoFisher Scientific).

Preparation of giant plasma membrane vesicles

Giant plasma membrane vesicles (GPMVs) were prepared according to published protocol (29) using 2 mM *N*-ethylmaleimide (Sigma Aldrich, Dorset, United Kingdom) as a vesiculating agent. HeLa cells were cultured in Dulbecco's Modified Eagle medium (Sigma Aldrich) with 10% fetal bovine serum (ThermoFisher Scientific) in T-25 flasks. The cells were brought to 80% confluence and incubated with 3–4 mL of vesiculating buffer for 90 min before gently collecting the buffer with floating GPMVs.

Hypergravity simulation

Hypergravity experiments were performed using the LDC facility (Zeugma; Tecnologia de Sistemas Industriais, Mafra, Portugal), housed at the European Space Agency Technology Centre (European Space Agency, Noordwijk, the Netherlands) (30). The imaging system described below was placed in a gondola on a 4-m arm and centrifuged to simulate hypergravity. The samples underwent two dynamic gravity-level ramps profiled as follows: 1) 1–15 × *g* at 1 × *g*/min, held for 30 min at 15 × *g* and 15–1 × *g* at 1 × *g*/min, held for 30 min at 1 × *g*; and 2) 1–15 × *g*

at 2 × *g*/min, held for 15 min at 15 × *g* and 15–1 × *g* at 2 × *g*/min, held for 15 min at 1 × *g*. The gondola was free to swing along the axis of the support arm; thus, the effective gravity vector was directly perpendicular to the sample plane.

Sample analysis system description

An inverted microscope (Axiovert 10; Zeiss, Cambridge, United Kingdom) was placed inside an outer gondola at the LDC (Fig. S1), and excitation was provided by a high-powered light-emitting diode (pE-4000; CoolLED, Andover, United Kingdom) tuned to 470 nm at 50% power. The microscope sits on the floor of the gondola and remains in place without further support because the gondola can swing freely outwards as the centrifuge speed increases (as described above), meaning that the effective gravity is always acting perpendicular to the gondola floor. Images were acquired using a Plan-Neofluor 63 × 1.25 NA oil immersion objective (Zeiss) and complementary metal-oxide semiconductor camera (Ximea MQ013RG-E2; Munster, Germany). The camera and light source were connected via a universal serial bus to a control computer housed in the central gondola of the centrifuge running custom-developed control software. A remote desktop connection from the LDC operator workstation to the control computer was then used to control the camera and light source and to enable real-time visualization of the sample. The light-emitting diode excitation light was fed to the microscope using an optical fiber and adaptor that were securely attached to the microscope. The fluorescence illumination was found not to be affected by gravity. At higher gravitational force (g) levels, the brightfield illumination became slightly distorted because of the standard mounting of the brightfield lamp flexing; however, brightfield images were only used for the initial visualization with no quantitative data gathered, so there was no need to reduce this distortion.

During observation, the sample was kept at 37°C using an objective heater (Okolab, Burlingame, CA) and a custom-built Peltier-controlled stage fitted into a Ludl-controlled xyz motorized stage (Fig. S1). The eight-well cover glass chamber was secured to the stage using industrial tape to ensure it remained fixed in place during acceleration and deceleration of the centrifuge. Again, because of the perpendicular effective gravitational force, no further movement of the sample chamber occurred. The stage position and microscope focus were controlled from the LDC operation workstation in addition to the excitation source and camera. The heated stage and objective heater were set up from inside the gondola before the experiment because further control during each run was not necessary and temperatures were monitored remotely.

Data analysis

Images were analyzed using Fiji and custom-built MATLAB software (The MathWorks, Natick, MA). To determine the gravity-induced trends in cellular viscosity, an average fluorescence intensity value was obtained over the whole field of view for each sample, which contained a minimum of two cells per field of view. The values were taken by using MATLAB software to crop images where necessary to remove noncellular artifacts before importing the images into Fiji and analyzing the fluorescence intensity of the whole field of view using the mean intensity value. The same field of view was followed over the gravity ramp, and the ramp was repeated at least five times for each cell line studied.

Statistical significance of the observed change in fluorescence intensity between different gravity conditions was found by using a standard 1-way paired Student's *t*-test on 10 individual cells, across 3 separate hypergravity runs. We have compared fluorescence intensity at four different conditions: 1) when the cells are at 1 × *g* before the gravitational loading, 2) when the cells are at 15 × *g* after 45 min, and 3) and 4) when control cells are held at 1 × *g* for 0 and 45 min. Before the statistical analysis, data were normalized by dividing the fluorescence intensity by the intensity at time zero.

Because the absolute values of viscosity are concentration dependent and the concentration of rotor 2 within each cell is not known, it was not possible to quantify a relative viscosity change based on changes in fluorescence intensity. Therefore, only the trends of fluorescence intensities (reflecting the trend in viscosity) throughout changing gravitational loading were interpreted.

RESULTS

The choice of molecular rotor 2

We have previously demonstrated that the family of boron-dipyrrin (BODIPY) molecular rotors can successfully stain organelles of a variety of mammalian cells in cellulo and in vivo (31). Alongside exhibiting a large dynamic range of fluorescence responses to viscosity, these dyes were successfully incorporated into a variety of cellular membranes. We have tested rotor 1 and a new dye rotor 2 (see Supporting Materials and Methods for detailed synthetic procedures and characterization), both containing a long hydrocarbon chain (Fig. 1 *a*). The two positive charges present in 2 were thought to aid its retention in a plasma membrane of cells and to improve water solubility by analogy with our other recently published molecular rotors (32). We rationalized that by increasing the number of carbons in the linking chain, we would increase the lipophilicity of the molecule and achieve better staining. This would therefore enable direct comparison with neutral rotor 1 (henceforth referred

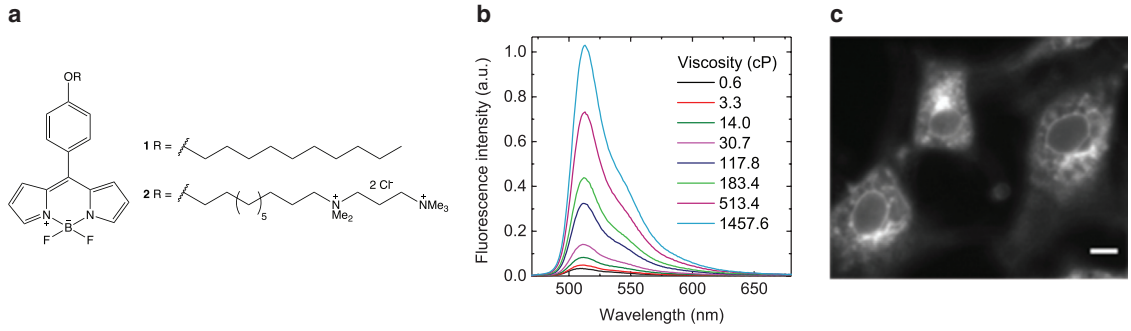

FIGURE 1 The molecular rotors 1 and 2. (*a*) The molecular structure of rotor 1 and rotor 2 is shown. (*b*) Fluorescence emission spectra of 2 in methanol/glycerol mixtures of varying concentrations with viscosities ranging from 0.6 to 1457.6 cP, excited at 450 nm, are shown. (*c*) A fluorescence intensity image showing representative staining of MC3T3-E1 cells with 2 at 1 × *g* (200-ms exposure), is shown. Scale bars, 10 μm. To see this figure in color, go online.

to as "1"), which was previously shown to internalize into SK-OV-3 and HeLa cells (20,31). 1 was successfully used in live cell studies at standard gravity conditions and is an attractive probe because of a large range of fluorescence responses between 0.6 and 1140 cP, as well as being temperature and polarity independent (33).

Before experiencing hypergravity conditions, cells were successfully stained with 1 and 2. However, with rotor 1, a rapid loss of fluorescence intensity was observed before initiation of the hypergravity profile, either because of a high rate of photobleaching of the dye by the excitation light or a lack of solubility in biological media, leading to dye aggregation; this fluorescence intensity loss was not seen with rotor 2 in which the fluorescence was found to remain constant over time at 1 × *g*. The fluorescence changes shown by rotor 1 made it unsuitable for qualitative comparison of viscosity, and so only rotor 2 was used in our hypergravity experiments (Fig. 1 *c*). Such a difference in fluorescence behavior is unsurprising because of the doubly positive charge of 2 in comparison to the neutrality of 1, which creates variation in the cellular localization of each dye. The higher hydrophobicity of 1 causes absorption solely into punctate cellular organelles where it easily accumulates to self-quenching concentrations, promoting photobleaching by the excitation light, whereas the less hydrophobic rotor 2 is internalized to more locations within live cells (Figs. 1 *c* and S2), limiting self-quenching and bleaching of the dye.

Given the promising cellular uptake and photostability, we tested the viscosity sensitivity of 2 to ensure it acted as a molecular rotor, with fluorescence emission intensity sensitive to local viscosity (Fig. 1 *b*). We measured the fluorescence emission spectra in mixtures of methanol and glycerol of various concentrations, with viscosities ranging between 0.6 (pure methanol) and 1457.6 cP (pure glycerol) at 20°C. The quantum yield was 0.16 in a 70:30 v/v glycerol/methanol mixture at 20°C (Fig. S3), and a significant increase in emission intensity with viscosity is apparent in Fig. 1 *b*. The peak fluorescence intensity at 511 nm increased more than 30 times over the viscosity span of 1–1000 cP (Fig. S4) demonstrating the significant viscosity sensitivity of the emission of rotor 2 in a viscosity range relevant for cellular membranes. For example, other BODIPY-based molecular rotors have reported average viscosity of 270 cP at 20°C in the plasma membranes of eukaryotic SK-OV-3 cells (34) and 2510 cP in eye lens cells (32). These values could be compared to a viscosity of approximately 1000 cP measured with molecular rotors in the inner membrane of *Escherichia coli* at 20°C, reporting an unusually high order of lipid organization (21). These measurements were performed under standard gravity conditions.

Viscosity changes in MC3T3-E1 cells under hypergravity

To investigate the changes in viscosity of a model mechanosensitive cell, MC3T3-E1 cells were stained with molecular rotor 2 and exposed to conditions of changing hypergravity, with images of fluorescence intensity recorded over time on the same field of view (Fig. 2). It is clear that the dye is retained intracellularly and its localization in the cells is unchanged with gravity.

The cells experienced a changing hypergravity profile, with the gravitational force increasing from 1 to 15 × *g* over a period of 15 min, followed by 30 min held at 15 × *g*, before decreasing from 15 to 1 × *g* over 15 min

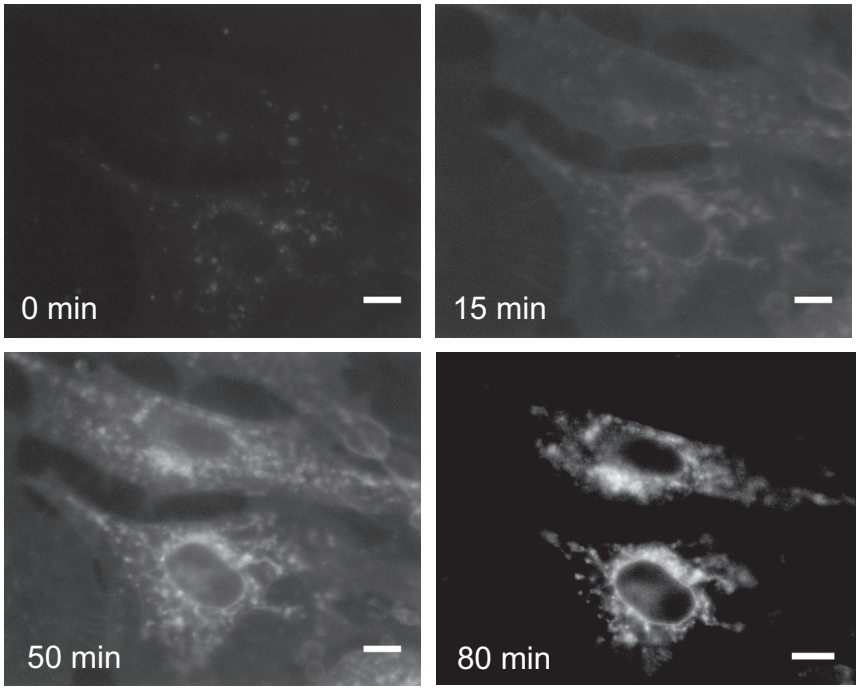

FIGURE 2 Fluorescence intensity images of MC3T3-E1 cells showing change in intensity of molecular rotor 2 at 1 × *g* (0 min), 15 × *g* (15 min), 10 × *g* (50 min), and 1 × *g* (80 min) using a 15-min ramp (200-ms exposure). Scale bars, 10 μm.

with a final hold at 1 × *g* for 30 min. Both low and high gravitational loads have previously caused cellular responses, with response times varying from minutes to several hours (35). Because viscosity responses under hypergravity have not been observed previously in this manner, a continuous gravity profile up to 15 × *g* gave certainty in obtaining a hypergravity-induced response, and cellular viability was monitored throughout. The MC3T3-E1 cells maintained a consistent, healthy cellular structure without swelling, blebbing, or fragmentation observed across the profile run (Fig. 2). Furthermore, there is no change of cellular localization of the rotor throughout the varying gravity profile, demonstrating that the fluorescence intensity change is correlated to cellular viscosity changes.

A strong positive correlation was displayed between the fluorescence intensity and gravitational force, which is in stark contrast to the lack of fluorescent intensity change observed when the cells are kept at a constant 1 × *g* (Fig. 3). Fig. S5 shows that the fluorescence increase we observed was reproducible and that this increase in fluorescence after exposure to hypergravity for 45 min was significant, with $p < 0.001$. A delay, or lag phase, is noticeable in Fig. 3 *a* between increasing the g level and the subsequent cellular viscosity increase, indicating an ∼10-min cellular response time to an altered gravitational environment. This lag time may be indicative of a biologically underpinned mechanism because any physical change would be instantaneous on these timescales (36).

As a control, we stained GPMVs with molecular rotor 2. GPMVs are vesicles derived directly from cells that have a membrane composition very similar to live cells; however, these structures lack cytoskeletons and biological machinery. GPMVs enable study of cellular membrane organization under controlled conditions, outside of living cells (29) and so act as a useful control when undertaking biological studies. We exposed the GPMVs to hypergravity in the LDC and measured the resulting fluorescence intensity change (Fig. S6). The lack of fluorescence change across the sample shows that any changes seen are related to a gravity-dependent biological effect, rather than a purely physical effect such as aggregation or disaggregation of the rotor. This result corresponds with our previously published data, which indicate that aggregation of BODIPY molecular rotors causes a decrease in fluorescence intensity, with the concentration threshold for significant aggregation well above the 5 μM concentration used in our experiments (33,37). Additionally, aggregation-like effects are not expected to be reversible, which is opposite to what is observed in our cellular experiments. Hence, physical effects such as dye aggregation will not meaningfully impact the fluorescence intensity change seen at our experimental conditions, and so, solely gravity-dependent biological effects are observed.

To probe the observed lag phase further, the g-level ramp rate was doubled; a lag phase of ∼10 min was again present (Fig. 3 *c*), indicating that the cellular response is time dependent and not dependent on reaching a threshold g level because, if so, we would only observe a response above this g-level value. A comparison of the rate of fluorescence intensity increase for each ramp using a straight-line approximation shows a rate difference that is not statistically significant. The similarity of these rates suggests that either the cellular response is insensitive to the rate of gravitational loading or another process is limiting the rate of the cellular response.

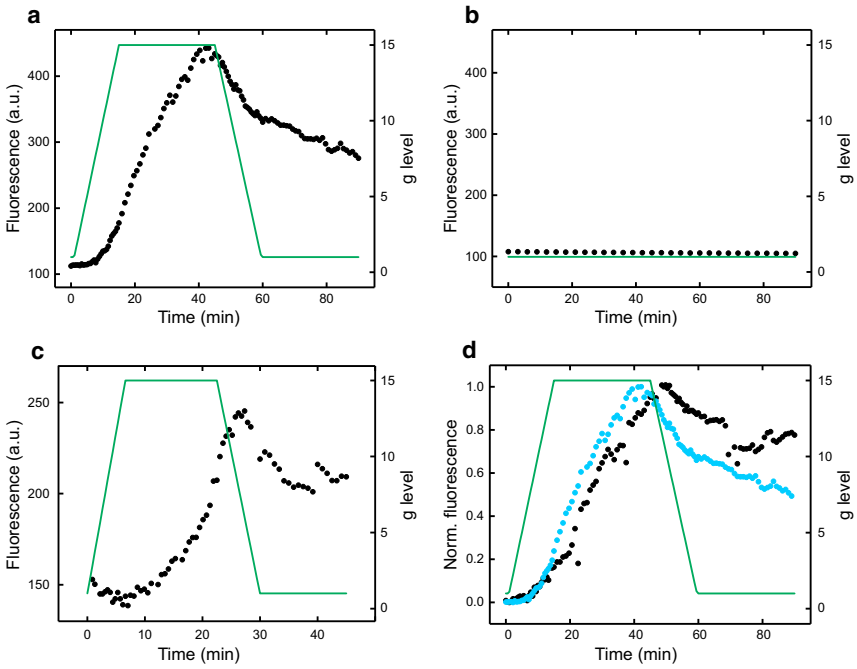

FIGURE 3 (*a*) Fluorescence response of 2 in MC3T3-E1 cells (*black*) as g level (*green*) is changed, with a 15-min ramp. (*b*) Control MC3T3-E1 cells showing no change in 2 fluorescence (*black*) as g level (*green*) is held at 1 × *g* are shown. (*c*) The fluorescence response of 2 in MC3T3-E1 cells (*black*) as g level (*green*) is changed with a 7.5-min ramp is shown. (*d*) A normalized fluorescence response of cells treated by previous hypergravity exposure and relaxation, before a second hypergravity exposure (*black*), compared with cells with no previous hypergravity exposure (*blue*) is shown. To see this figure in color, go online.

Upon gravitational force unloading, the fluorescence intensity decreases in all traces (Fig. 3), giving further evidence that the observed change in intensity is due to a changing g level rather than a dye relocalization. However, the fluorescence intensity decreases at a slower rate than the previous increase, meaning the initial fluorescence intensity level present before gravitational loading was not reached. We can therefore conclude that upon removal of hypergravity conditions, MC3T3 cells will relax toward their "prehypergravity" state; however, this relaxation will take some time (on the order of hours).

To confirm full cellular relaxation after hypergravity exposure, an unstained MC3T3 cell sample was ramped as previously stated, then held at 1 × *g* for 3 h, stained, and ramped again. These data were then compared with a cell sample that had not previously experienced hypergravity (Fig. 3 *d*). Little difference is observed between the "hypergravity-treated" and untreated cells, with the same lag phase and similar rates of fluorescence intensity increase for each sample. This similarity indicates that no permanent changes to the cells occur upon application of abnormal gravity conditions up to 15 × *g*.

Viscosity changes in HUVECs under hypergravity

Although MC3T3-E1 cells provide a model for viscosity changes undergone by structural oriented cells and connective tissue in hypergravity, this model cannot be applied to other tissue types. To investigate the effect of gravitational loading on epithelial tissue, HUVECs were incubated with rotor 2 and imaged in response to hypergravity (Fig. 4 *b*). In vivo, this cell type has developed mechanisms to adapt to pressure variations in blood vessels to prevent disease such as atherosclerosis (26,38). Furthermore, viscosity changes in blood plasma have been implicated in, for example, diabetes (39) and Alzheimer's disease (39). Hence a nonnegligible response to hypergravity is expected in the HUVEC cell line.

The fluorescence intensity in HUVECs correlated positively with the gravitational field (Fig. 4, *a* and *c*). In contrast to MC3T3-E1 cells, the late-stage decrease occurs at a rate similar to the increase, indicating that HUVECs are quickly able to relax back to their original, prehypergravity state. This effective relaxation after gravitational unloading could be symptomatic of the ability of HUVECs to adapt rapidly to changes in shear stress and pressure in blood vessels.

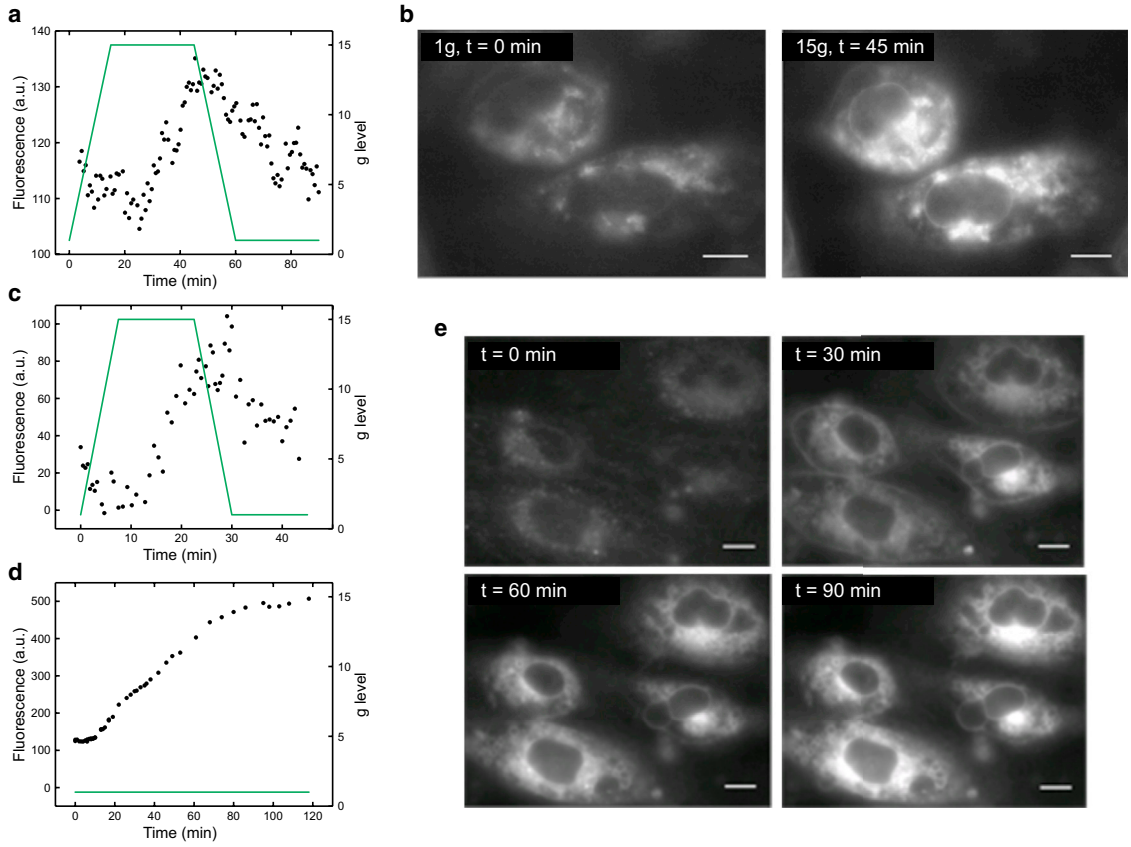

FIGURE 4 (*a*) Fluorescence response of 2 in HUVECs (*black*) as g level (*green*) is changed, with a 15-min ramp. (*b*) Fluorescence images of HUVECs showing change in intensity of 2 at 1 × *g* (*t* = 0 min) and 15 × *g* (*t* = 45 min) during a 15-min ramp (200-ms exposure), are shown. (*c*) The fluorescence response of 2 in HUVECs (*black*) as g level (*green*) is changed with a 7.5-min ramp is shown. (*d*) Control HUVECs showing an increase in 2 fluorescence intensity (*black*) as g level (*green*) is held at 1 × *g* are shown. (*e*) Fluorescence images of HUVECs showing change in intensity of 2 at 1 × *g* at various time points are shown. Scale bars, 10 μm. To see this figure in color, go online.

Similar to MC3T3-E1 cells, a delayed response of approximately 20 min occurs between gravitational loading and the cellular viscosity increasing. Similarly to what was used previously, we doubled the g-level ramp rate, going from 1 to 15 $\times$ g in 7.5 min (Fig. 4 *c*) (initially 15 min was taken), to investigate the response time further. Unlike with the MC3T3-E1 cells, the lag phase changed with an altered ramp rate; the delay halved to 10 min with a doubled gravitational ramp rate. This halving therefore indicates HUVECs produce a cellular response caused by g level, as confirmed by the initial fluorescence intensity decrease seen in this delay time. The intensity decrease may be indicative of an instantaneous physical response to prevent cell damage while a biological response is being prepared or the presence of a g-level threshold below which a cellular response does not occur.

As a control, we measured the fluorescence intensity of cells in the LDC for 2 h at 1 $\times$ g. It was expected that there would be no fluorescence change; however, a distinct increase in fluorescence intensity was seen (Fig. 4, *d* and *e*). Because the staining media was replaced before any fluorescence measurements occurred, continuous dye accumulation or aggregation inside the cell was not causing this increase; changes of fluorescence intensity due to dye movement could be addressed by measuring fluorescence lifetime. However, this setup was not possible within the LDC.

Although there is an intensity increase during the 1 $\times$ g control, it does not correspond with the trend seen when the cells are exposed to hypergravity; thus, we conclude that a gravitational response must be occurring in addition to a steady fluorescence increase seen at 1 $\times$ g. In both the 15 min ramp and the control experiments, cell blebbing and abnormal nuclear shape can be seen at later incubation times (Fig. 4, *b* and *e*), which are both signs of apoptosis and/or necrosis. Although the cells are not in optimal health, there is still a clear biological response to both gravity loading and unloading, providing evidence for hypergravity measurements to understanding the interactions of individual endothelial cells with the local vascular environment.

DISCUSSION

Viscosity is a highly significant property of the cell. It provides an intrinsic control mechanism for the movement of proteins (e.g., within the cytoplasm (40) or within plasma membrane (41)), controlling cell diffusion, gene expression, signaling, and structure. Yet probing the mechanisms that cause changed viscosity and its downstream effect on cellular function still poses significant challenges. Directly measuring membrane viscosity within cells has only recently become achievable (21), and achieving abnormal single cell conditions without the addition of a molecular agent requires external influences, such as gravity loading; this study is the first, to our knowledge, to combine the application of hypergravity to a cell with fluorescent molecular rotors to enable real-time imaging of single cell viscosity changes.

We have designed several molecular rotors to specifically incorporate in lipid-rich cell domains such as lipid membranes. Both molecular dynamic simulations and studies with phase-separated giant unilamellar vesicles, which act as mimetics for the cellular lipid membrane, demonstrate the ability for the molecular rotor to insert into the cell membrane and to accurately report on its immediate viscosity with fluorescence (42). In our chosen cell types, 2 is shown to internalize and stain both the cellular membrane and internal lipid-rich domains; hence, the internal organelles' membrane viscosity can be imaged.

Although fluorescence lifetime imaging microscopy can be used to generate concentration-independent quantitative viscosity measurements over a heterogeneous sample (20,23), a fluorescence lifetime imaging microscopy setup is required, which is not practically possible to house within the LDC. An equally valid approach can be employed using fluorescence intensity measurements alone (34), provided the concentration of a fluorophore does not change during the experiment. Although the concentration of molecular rotor within the membranes is unknown, it can be assumed that the concentration does not change over changing gravitational level because no excess rotor is present in the external medium and so no migration of rotor within the cell occurs. Relative changes in viscosity can therefore be compared to evaluate the effect of hypergravity conditions on cells.

Although other methods for creating hypergravity conditions, such as a parabolic flight, cause cellular responses (43), a viable method for measuring single cell viscosity changes with fluorescence microscopy is not available, and the level of hypergravity loading possible is low. By using the LDC, we were able to centrifuge a fluorescence microscope and therefore directly image single cells while they were being exposed to an increasing gravitational load. Because the LDC has a much larger diameter than that of common laboratory centrifuges, it also minimized the relative influence of shear force acting upon the sample. In centrifuges, inertial shear forces act perpendicular to the gravitational force and could elicit responses from the cells (44). It has previously been shown that fluid shear force applied to endothelial cells causes a change in the transcriptional activity within the cell, with genes associated with controlling the cytoskeletal structure being up- or downregulated depending on the flow of the stress (38). An LDC significantly reduces inertial shear force and therefore prevents cellular mechanosensing occurring from stresses other than hypergravity alone (44).

One common cell line used in gravisensing research is MC3T3-E1, a mouse preosteoblast immortalized cell line. This cell type is used as a model system in bone biology, specifically in cell mechanosensing of force and strain because of its physiological relevance and homogeneous character (45). Under microgravity, disruption of the osteoblast

cytoskeleton has been observed via an enlarged nucleus (46). Because the cytoskeleton is well linked to cellular function and morphology (47), it is possible that the increase in cellular viscosity seen upon gravitational loading is caused by a cytoskeletal stress response and regulation.

Although MC3T3-E1 cells provide a firm foundation for observing viscosity changes under hypergravity with molecular rotors, employing this system in a human cell may enable research into how cellular viscosity is impacted by disease and hence the pathogenesis of certain disease types. The circulatory system is implicated in diseases from cardiovascular disorders to diabetes, so endothelial cells may provide information for the mechanism of the proliferation of such malfunctions. The mechanosensitivity of endothelial cells allows them to combat and respond to changes in the stress of their surroundings; however, a variation in such response is a key feature in many diseases (48). Modulation of endothelial cell functions is therefore a crucial study area for determining their role in pathogenesis pathways, and observing viscosity changes in these cells provides a clear idea for how this pathogenesis occurs on a single cell level.

HUVEC is an endothelial cell line often used as model systems for endothelial cell pathways. Because this cell type solely lines the interior of blood vessels, aiding blood pressure control, HUVECs exhibit a clear response to changes in blood shear stress and viscosity (26). This response to mechanical loading, combined with previously observed responses to alterations in gravity (7,49), further support the changes in cellular viscosity seen here under hypergravity. The sensitivity of the cytoskeleton to gravitational changes is well known; gravitational unloading in HUVECs has been shown to cause a disorganization of the cytoskeleton via a transcriptional regulation of actin (50), and the rapid nature of this sensing has been demonstrated as causing significant alterations in a short time period (51). Furthermore, when human thyroid cancer cells were exposed to hypergravity, an upregulation of actin expression was seen (51); because these proteins contribute to the structure of the cell cytoskeleton and plasma membrane (52), it is likely that the increase in viscosity seen in the cellular membrane is due to an increased organization of these actin-based structures, activated by the higher actin expression under hypergravity. Furthermore, alterations in the rigidity of the cell under simulated microgravity were found to not take place instantaneously, which is consistent with the initial lag in fluorescence intensity increase seen in our cells (53).

In addition to biological causes of viscosity changes being demonstrated, it has previously been shown that the cellular membrane also gives a physical response to abnormal gravity conditions. Phospholipid vesicles were demonstrated to undergo an increase and decrease in membrane viscosity under hyper- and microgravity, respectively (9). It can be hypothesized that at higher gravities, the membrane becomes more compressed and so has a reduced fluidity, resulting in an increased bilayer viscosity. The numerically small variation in vesicular viscosity seen may indicate why only a lag response was detected in our system; it is possible that the strong cellular biological response was much greater than any instantaneous physical response within the membrane, such as lipid compression or packing changes (54), and so the much smaller lipid-driven changes were not observed.

It has previously been shown that lipid membranes respond within 5 ms to physical perturbations, such as pressure (55). Because membrane viscosity is primarily dominated by interactions between lipid hydrocarbon chains, any physical response is likely to occur near instantly; slower physical changes such as large movement or physical reorganization of intracellular organelles are highly unlikely. The cellular membrane viscosity can be modulated through biological pathways that do not require full synthesis and insertion of lipids into the bilayer; variations in squalene concentration in the membrane enact a viscosity change as a function of environmental stress (56). In the same way, cytosolic viscosity could be modulated by moving relatively small molecule components between compartments. Both the lack of instantaneous response and possibility of fast biological modulations lead to the assumption of a biologically driven mechanism being observed in each cell type.

The large differences in fluorescence intensity between HUVECs and MC3T3 cells may be due to physical variations within the membrane. The lipid-protein composition of each cellular membrane is known to significantly affect the magnitude of the response to gravity variation (9). Changes in the membrane composition as a response to high pressure, such as an increase in the concentration of unsaturated fatty acids, vary with cell type (57) and so differing magnitudes of viscosity changes would be expected under hypergravity.

CONCLUSIONS

We have clearly demonstrated a correlation for the impact of hypergravity loading and unloading on cellular viscosity. These findings indicate an adaptive response of both preosteoblast bone cells and endothelial cells to dynamic changes in gravitational force, possibly due to restructuring of the cytoskeleton. Further studies should be employed to confirm the mechanisms of such a response. This work may enable the development of novel approaches to explore pathogenesis pathways of vascular diseases, as well as provide a foundation for further investigation of anisotropic conditions on lipid biomembranes.

SUPPORTING MATERIAL

Supporting Material can be found online at https://doi.org/10.1016/j.bpj.2019.03.038.

AUTHOR CONTRIBUTIONS

E.M.W. and P.G. conducted hypergravity work and data analysis and participated in writing the final manuscript. J.E. conducted hypergravity work and data analysis. I.L.D. synthesized the molecular rotors and participated in writing the final manuscript. M.K. characterized rotor 2 and participated in writing the final manuscript. J.J.W.A.v.L operated the LDC facility. J.J.W.A.v.L., N.J.B., and M.K.K. conceived the study and provided project oversight. All authors gave final approval for publication.

ACKNOWLEDGMENTS

The authors thank Alan Dowson (European Space Agency Technology Centre, Noordwijk, the Netherlands) for technical support. J.E. thanks Jens-Uwe Sommer (Leibniz Institute of Polymer Research Dresden).

The authors acknowledge the Spin Your Thesis! 2017 campaign, organized by European Space Agency Education, for supporting this research and European Space Agency grant/contract 4000107455/12/NL/PA awarded to J.J.W.A.v.L. M.K.K. is grateful to the Engineering and Physical Sciences Research Council for the Career Acceleration Fellowship (EP/I003983/1). N.J.B. is grateful to the Engineering and Physical Sciences Research Council for the support of program grant EP/J017566/1.

REFERENCES

1. Bizzarri, M., M. Monici, and J. J. van Loon. 2015. How microgravity affects the biology of living systems. *Biomed Res. Int.* 2015:863075.
2. Feric, M., and C. P. Brangwynne. 2013. A nuclear F-actin scaffold stabilizes ribonucleoprotein droplets against gravity in large cells. *Nat. Cell Biol.* 15:1253–1259.
3. Demets, R. 2011. Biology on sounding rockets: History, requirements, results and scientific interpretation. *In* Proceedings of the 20th Symposium on European Rocket and Balloon Programmes and Related Research. L. Ouwehand, ed. ESA SP-700, pp. 63–66.
4. Huang, Y., Z. Q. Dai, …, Y. H. Li. 2009. Gravity, a regulation factor in the differentiation of rat bone marrow mesenchymal stem cells. *J. Biomed. Sci.* 16:87.
5. Vorselen, D., W. H. Roos, …, J. J. van Loon. 2014. The role of the cytoskeleton in sensing changes in gravity by nonspecialized cells. *FASEB J.* 28:536–547.
6. Matía, I., F. González-Camacho, …, F. Javier Medina. 2010. Plant cell proliferation and growth are altered by microgravity conditions in spaceflight. *J. Plant Physiol.* 167:184–193.
7. Costa-Almeida, R., D. T. Carvalho, …, P. L. Granja. 2016. Effects of hypergravity on the angiogenic potential of endothelial cells. *J. R. Soc. Interface.* 13:20160688.
8. Chebli, Y., L. Pujol, …, A. Geitmann. 2013. Cell wall assembly and intracellular trafficking in plant cells are directly affected by changes in the magnitude of gravitational acceleration. *PLoS One.* 8:e58246.
9. Sieber, M., W. Hanke, and F. P. M. Kohn. 2014. Modification of membrane fluidity by gravity. *Open J. Biophys.* 4:105–111.
10. Kuimova, M. K., G. Yahioglu, and P. R. Ogilby. 2009. Singlet oxygen in a cell: spatially dependent lifetimes and quenching rate constants. *J. Am. Chem. Soc.* 131:332–340.
11. Zheng, K., T. P. Jensen, …, D. A. Rusakov. 2017. Nanoscale diffusion in the synaptic cleft and beyond measured with time-resolved fluorescence anisotropy imaging. *Sci. Rep.* 7:42022.
12. Kato, G. J., M. H. Steinberg, and M. T. Gladwin. 2017. Intravascular hemolysis and the pathophysiology of sickle cell disease. *J. Clin. Invest.* 127:750–760.
13. Agrawal, R., T. Smart, …, C. Pavesio. 2016. Assessment of red blood cell deformability in type 2 diabetes mellitus and diabetic retinopathy by dual optical tweezers stretching technique. *Sci. Rep.* 6:15873.
14. Irace, C., C. Carallo, …, A. Gnasso. 2014. Blood viscosity in subjects with normoglycemia and prediabetes. *Diabetes Care.* 37:488–492.
15. Kuter, K., M. Kratochwil, …, N. A. Dencher. 2016. Adaptation within mitochondrial oxidative phosphorylation supercomplexes and membrane viscosity during degeneration of dopaminergic neurons in an animal model of early Parkinson's disease. *Biochim. Biophys. Acta.* 1862:741–753.
16. Eckmann, J., L. E. Clemens, …, G. P. Eckert. 2014. Mitochondrial membrane fluidity is consistently increased in different models of Huntington disease: restorative effects of olesoxime. *Mol. Neurobiol.* 50:107–118.
17. Munder, T., A. Pfeffer, …, C. Klein. 2018. MR elastography detection of early viscoelastic response of the murine hippocampus to amyloid β accumulation and neuronal cell loss due to Alzheimer's disease. *J. Magn. Reson. Imaging.* 47:105–114.
18. Cognet, L., C. Leduc, and B. Lounis. 2014. Advances in live-cell single-particle tracking and dynamic super-resolution imaging. *Curr. Opin. Chem. Biol.* 20:78–85.
19. Klymchenko, A. S., and R. Kreder. 2014. Fluorescent probes for lipid rafts: from model membranes to living cells. *Chem. Biol.* 21:97–113.
20. Kuimova, M. K., G. Yahioglu, …, K. Suhling. 2008. Molecular rotor measures viscosity of live cells via fluorescence lifetime imaging. *J. Am. Chem. Soc.* 130:6672–6673.
21. Mika, J. T., A. J. Thompson, …, M. K. Kuimova. 2016. Measuring the viscosity of the Escherichia coli plasma membrane using molecular rotors. *Biophys. J.* 111:1528–1540.
22. Kuimova, M. K. 2012. Mapping viscosity in cells using molecular rotors. *Phys. Chem. Chem. Phys.* 14:12671–12686.
23. Dent, M. R., I. López-Duarte, …, M. K. Kuimova. 2016. Imaging plasma membrane phase behaviour in live cells using a thiophene-based molecular rotor. *Chem. Commun. (Camb.).* 52:13269–13272.
24. Chambers, J. E., M. Kubankova, …, M. K. Kuimova. 2018. An optical technique for mapping microviscosity dynamics in cellular organelles. *ACS Nano.* 12:4398–4407.
25. Searby, N. D., C. R. Steele, and R. K. Globus. 2005. Influence of increased mechanical loading by hypergravity on the microtubule cytoskeleton and prostaglandin E2 release in primary osteoblasts. *Am. J. Physiol. Cell Physiol.* 289:C148–C158.
26. Davies, P. F. 2009. Hemodynamic shear stress and the endothelium in cardiovascular pathophysiology. *Nat. Clin. Pract. Cardiovasc. Med.* 6:16–26.
27. Umberger, J. Q., and V. K. LaMer. 1945. The kinetics of diffusion controlled molecular and ionic reactions in solution as determined by measurements of the quenching of fluorescence. *J. Am. Chem. Soc.* 67:1099–1109.
28. Afshar Ghotli, R., A. R. Abdul Aziz, …, M. K. Aroua. 2015. Selected physical properties of binary mixtures of crude glycerol and methanol at various temperatures. *J. Ind. Eng. Chem.* 21:1039–1043.
29. Sezgin, E., H. J. Kaiser, …, I. Levental. 2012. Elucidating membrane structure and protein behavior using giant plasma membrane vesicles. *Nat. Protoc.* 7:1042–1051.
30. van Loon, J. J. W. A., J. Krausse, …, P. Schiller. 2008. The Large Diameter Centrifuge, LDC, for Life and Physical Sciences and Technology. *In* Life Sp. Life Earth. L. Ouwehand, ed. ESA-SP.
31. Shimolina, L. E., M. A. Izquierdo, …, M. K. Kuimova. 2017. Imaging tumor microscopic viscosity in vivo using molecular rotors. *Sci. Rep.* 7:41097.
32. Sherin, P. S., I. López-Duarte, …, M. K. Kuimova. 2017. Visualising the membrane viscosity of porcine eye lens cells using molecular rotors. *Chem. Sci. (Camb.).* 8:3523–3528.
33. Hosny, N. A., G. Mohamedi, …, M. K. Kuimova. 2013. Mapping microbubble viscosity using fluorescence lifetime imaging of molecular rotors. *Proc. Natl. Acad. Sci. USA.* 110:9225–9230.
34. López-Duarte, I., T. T. Vu, …, M. K. Kuimova. 2014. A molecular rotor for measuring viscosity in plasma membranes of live cells. *Chem. Commun. (Camb.).* 50:5282–5284.

35. Maier, J. A., F. Cialdai, …, L. Morbidelli. 2015. The impact of microgravity and hypergravity on endothelial cells. *Biomed Res. Int.* 2015:434803.

36. Brooks, N. J. 2014. Pressure effects on lipids and bio-membrane assemblies. *IUCrJ.* 1:470–477.

37. Wu, Y., M. Stefl, …, M. K. Kuimova. 2013. Molecular rheometry: direct determination of viscosity in Lo and Ld lipid phases via fluorescence lifetime imaging. *Phys. Chem. Chem. Phys.* 15:14986–14993.

38. Dardik, A., L. Chen, …, B. E. Sumpio. 2005. Differential effects of orbital and laminar shear stress on endothelial cells. *J. Vasc. Surg.* 41:869–880.

39. Zubenko, G. S., U. Kopp, …, L. L. Firestone. 1999. Platelet membrane fluidity individuals at risk for Alzheimer's disease: a comparison of results from fluorescence spectroscopy and electron spin resonance spectroscopy. *Psychopharmacology (Berl.).* 145:175–180.

40. Kalwarczyk, T., N. Ziebacz, …, R. Hołyst. 2011. Comparative analysis of viscosity of complex liquids and cytoplasm of mammalian cells at the nanoscale. *Nano Lett.* 11:2157–2163.

41. Renner, M., D. Choquet, and A. Triller. 2009. Control of the postsynaptic membrane viscosity. *J. Neurosci.* 29:2926–2937.

42. Dent, M. R., I. López-Duarte, …, M. K. Kuimova. 2015. Imaging phase separation in model lipid membranes through the use of BODIPY based molecular rotors. *Phys. Chem. Chem. Phys.* 17:18393–18402.

43. Wehland, M., X. Ma, …, D. Grimm. 2013. The impact of altered gravity and vibration on endothelial cells during a parabolic flight. *Cell. Physiol. Biochem.* 31:432–451.

44. van Loon, J. J., E. H. Folgering, …, T. H. Smit. 2003. Inertial shear forces and the use of centrifuges in gravity research. What is the proper control? *J. Biomech. Eng.* 125:342–346.

45. Czekanska, E. M., M. J. Stoddart, …, J. S. Hayes. 2012. In search of an osteoblast cell model for in vitro research. *Eur. Cell. Mater.* 24:1–17.

46. Nabavi, N., A. Khandani, …, R. E. Harrison. 2011. Effects of microgravity on osteoclast bone resorption and osteoblast cytoskeletal organization and adhesion. *Bone.* 49:965–974.

47. Starr, D. A. 2007. Communication between the cytoskeleton and the nuclear envelope to position the nucleus. *Mol. Biosyst.* 3:583–589.

48. Rajendran, P., T. Rengarajan, …, I. Nishigaki. 2013. The vascular endothelium and human diseases. *Int. J. Biol. Sci.* 9:1057–1069.

49. Szulcek, R., J. van Bezu, …, G. P. van Nieuw Amerongen. 2015. Transient intervals of hyper-gravity enhance endothelial barrier integrity: impact of mechanical and gravitational forces measured electrically. *PLoS One.* 10:e0144269.

50. Carlsson, S. I., M. T. Bertilaccio, …, J. A. Maier. 2003. Endothelial stress by gravitational unloading: effects on cell growth and cytoskeletal organization. *Biochim. Biophys. Acta.* 1642:173–179.

51. Corydon, T. J., S. Kopp, …, D. Grimm. 2016. Alterations of the cytoskeleton in human cells in space proved by life-cell imaging. *Sci. Rep.* 6:20043.

52. Fletcher, D. A., and R. D. Mullins. 2010. Cell mechanics and the cytoskeleton. *Nature.* 463:485–492.

53. Janmaleki, M., M. Pachenari, …, A. Sanati-Nezhad. 2016. Impact of simulated microgravity on cytoskeleton and viscoelastic properties of endothelial cell. *Sci. Rep.* 6:32418.

54. Brooks, N. J., O. Ces, …, J. M. Seddon. 2011. Pressure effects on lipid membrane structure and dynamics. *Chem. Phys. Lipids.* 164:89–98.

55. Winter, R., and C. Jeworrek. 2009. Effect of pressure on membranes. *Soft Matter.* 5:3157.

56. Oger, P. M., and A. Cario. 2013. Adaptation of the membrane in Archaea. *Biophys. Chem.* 183:42–56.

57. Mota, M. J., R. P. Lopes, …, J. A. Saraiva. 2013. Microorganisms under high pressure–adaptation, growth and biotechnological potential. *Biotechnol. Adv.* 31:1426–1434.

Biophysical Journal, Volume *116*

Supplemental Information

Measuring Intracellular Viscosity in Conditions of Hypergravity

Emma M. Woodcock, Paul Girvan, Julia Eckert, Ismael Lopez-Duarte, Markéta Kubánková, Jack J.W.A. van Loon, Nicholas J. Brooks, and Marina K. Kuimova

1. Supplementary Figures

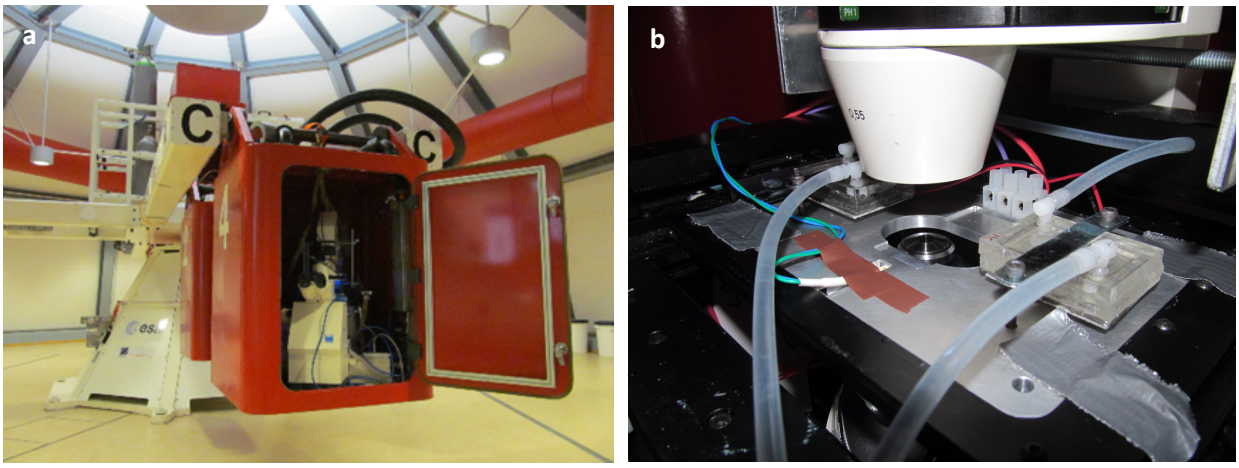

Figure S1. Images of the experimental setup. (a) The inverted microscope mounted inside an LDC gondola, which also contained the excitation source and camera. (b) View of the custom-built microscope stage showing the water-cooled portion of the peltier modules. A recess was machined into the microscope stage to tightly hold the sample in place.

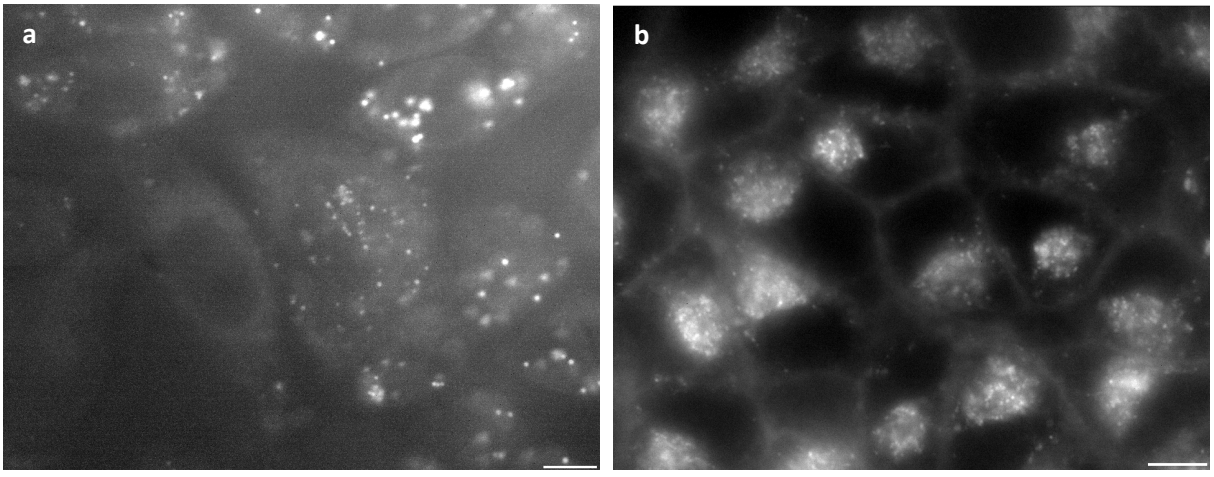

Figure S2. Fluorescence intensity images, acquired on an inverted microscope attached to a cooled system, of HeLa cells stained with (a) rotor **1** at 1g, 200 ms exposure; and (b) rotor **2** at 1 g, 200 ms exposure. Scale bars: 10 µm.

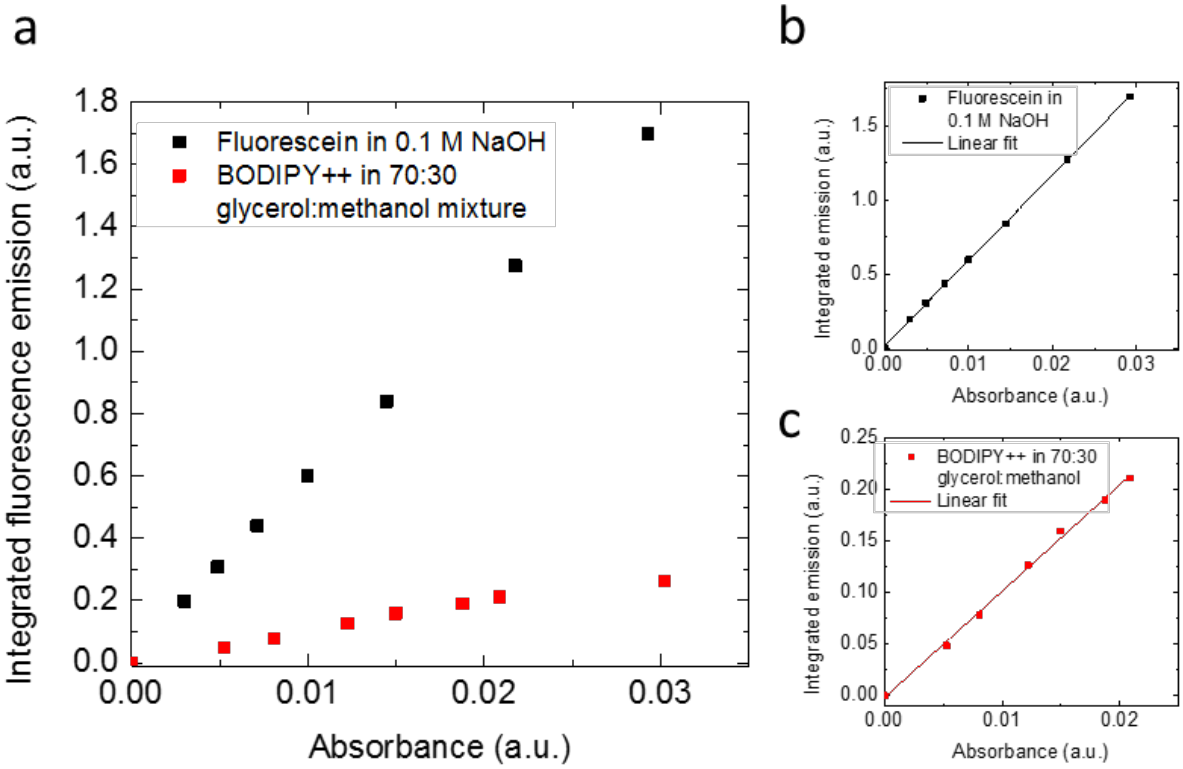

Figure S3. Determination of the quantum yield of rotor **2** in a 70:30 v/v mixture of glycerol/methanol at 20°C. The quantum yield of **2** was estimated by fitting the absorbance vs. integrated fluorescence emission intensity to a linear model and comparing the slope with the linear fit of absorbance vs. integrated fluorescence emission intensity of the reference dye fluorescein. (a) Absorbance vs. integrated fluorescence emission intensity of fluorescein in 0.1 M NaOH and **2** in 70:30 MeOH:glycerol mixture. The quantum yield was obtained via equation $\Phi_X = \Phi_{ST}\left(\frac{Grad_X}{Grad_{ST}}\right)\left(\frac{\eta_X{}^2}{\eta_{ST}{}^2}\right)$ where according to the linear fitting shown in panels (b, c), the numerical values of slopes are (b) $Grad_{ST}$ = 57.56 for fluorescein and (c) $Grad_x$ = 10.30 for **2**. Details of the calculation are found in the Methods section of the main text.

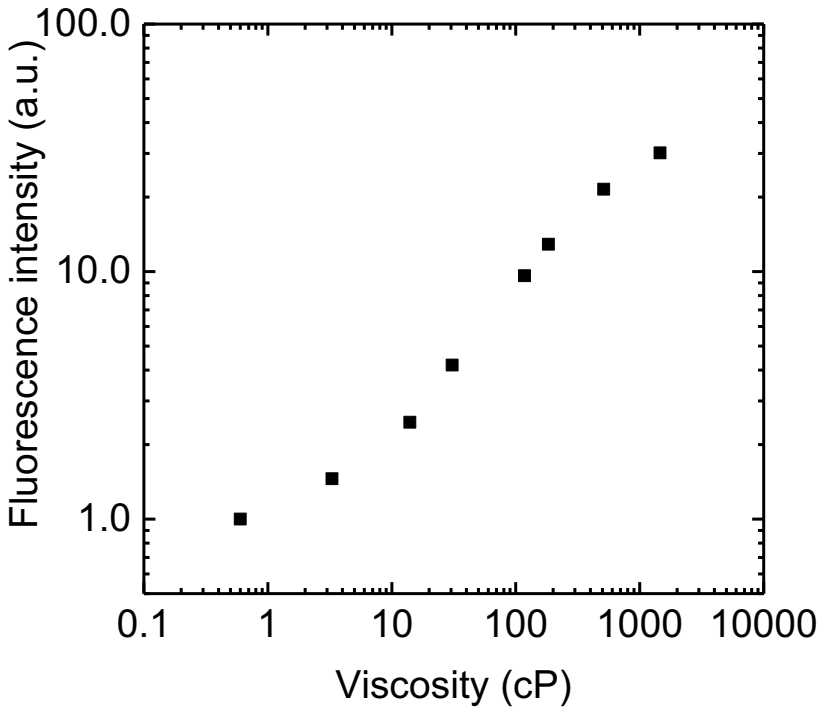

Figure S4. The viscosity sensitivity of molecular rotor **2** fluorescence. Rotor **2** emission intensity at 511 nm as a function of viscosity of methanol/glycerol mixtures, demonstrating over 30 times increase of fluorescence intensity over viscosities of 1 – 1 000 cP.

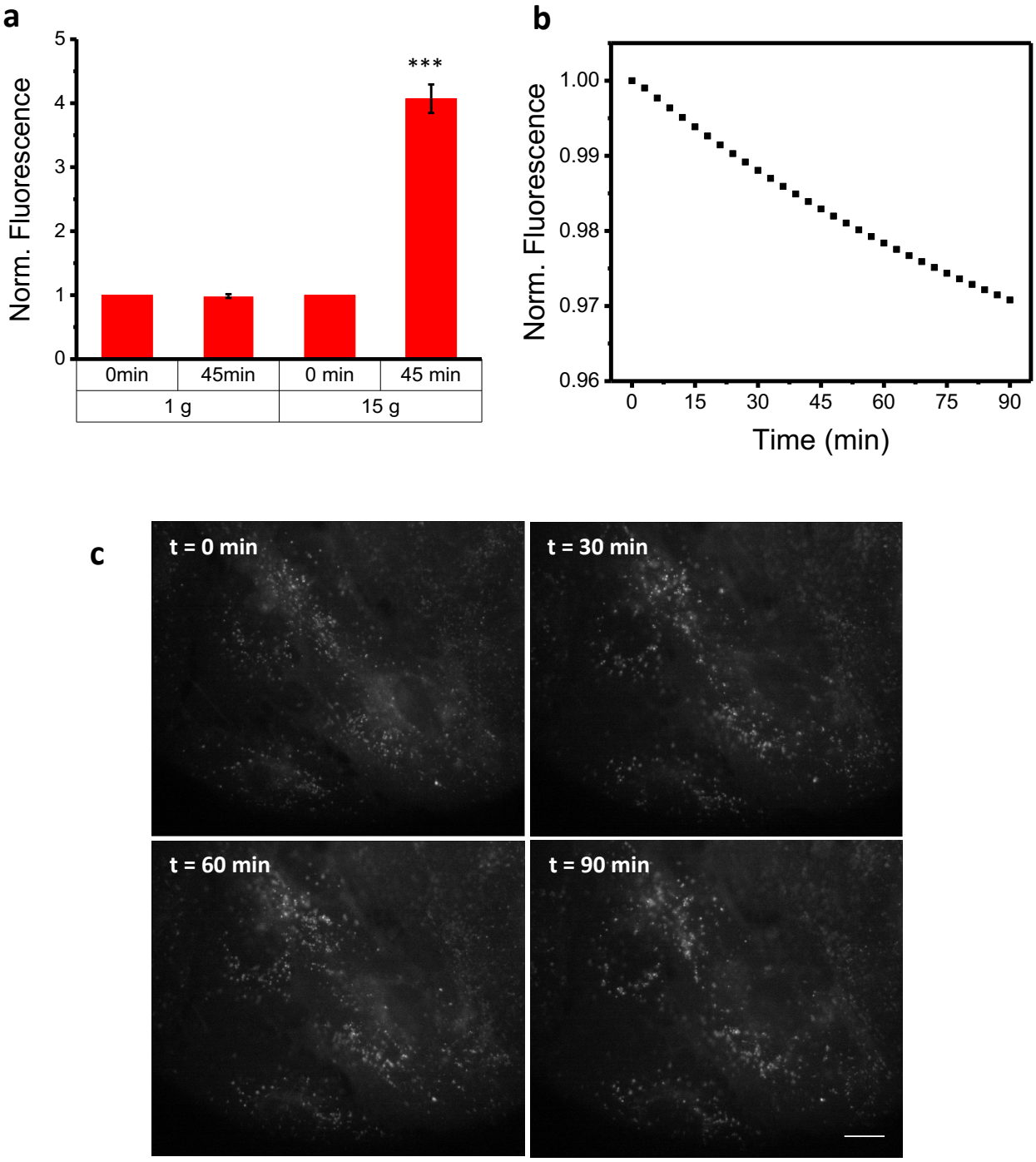

Figure S5. Fluorescence intensity changes of **2** in MC3T3-E1 cells. (a) Average relative fluorescence intensity change in individual cells at 1 g over 45 min and when exposed to hypergravity (15 g) across a 45 min profile, p = 0.001, n = 10, error bars show standard deviation across measured cells. p-value calculated using one way paired Student's t-test. (b) Relative fluorescence intensity change at 1 g over 90 min, showing a minimal total photobleaching effect of 3%. (c) Fluorescence images of cells at 1 g over 90 min. Scale bar 10 µm.

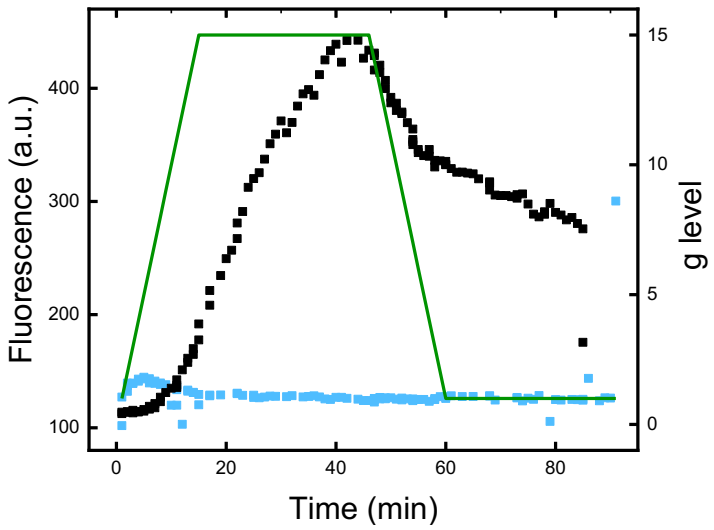

Figure S6. Fluorescence intensity changes of **2** in GPMVs (blue) as g level (green) is changed, with a 15 min ramp. Fluorescence response of **2** in MC3T3-E1 cells (black) is shown for comparison.

2. Synthesis and compound characterization

2.1 General Materials and Methods

The manipulation of all air and/or water sensitive compounds was carried out using standard inert atmosphere techniques. All chemicals were used as received from commercial sources without further purification. Anhydrous solvents were used as received from commercial sources. Analytical thin layer chromatography (TLC) was carried out on Merck® aluminium backed silica gel 60 GF254 plates and visualization when required was achieved using UV light or I_2. Flash column chromatography was performed on silica gel 60 GF254 using a positive pressure of nitrogen with the indicated solvent system. Where mixtures of solvents were used, ratios are reported by volume. Nuclear magnetic resonance spectra were recorded on 400 MHz spectrometers at ambient probe temperature. Chemical shifts for ^{1}H NMR spectra are recorded in parts per million from tetramethylsilane with the solvent resonance as the internal standard (chloroform: δ = 7.26 ppm or methanol: δ = 3.31 ppm). ^{13}C NMR spectra were recorded with complete proton decoupling. Chemical shifts are reported in parts per million from tetramethylsilane with the solvent resonance as the internal standard ($^{13}CDCl_3$: 77.0 ppm or $^{13}CD_3OD$: 49.00 ppm). ^{19}F NMR spectra were recorded with complete proton decoupling. Chemical shifts are reported in parts per million referenced to the standard hexafluorobenzene: −164.9 ppm. Mass spectra were carried out using ElectroSpray Ionization (ESI), and only molecular ions are reported.

2.2 Synthetic Procedures

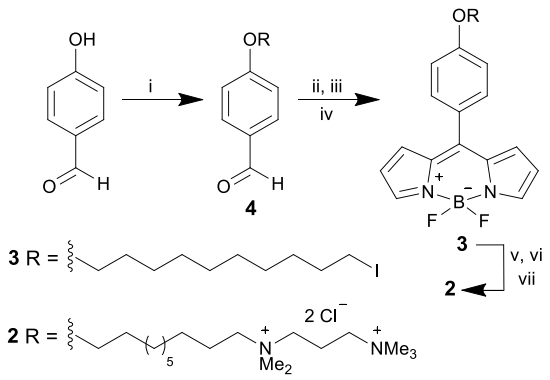

Scheme 1. Synthesis of **Rotor 2**: (i) 1,10-Diiododecane, K_2CO_3, DMF, Yield: 65%; (ii) neat pyrrole, TFA, Yield: 94%; (iii) DDQ, CH_2Cl_2 and then (iv) $BF_3{\cdot}(OEt_2)_2$, Et_3N, CH_2Cl_2, Yield: 24%;[1] (v) *N,N,N′,N′*-tetramethyl-1,3-propanediamine, THF, RT and then (vi) CH_3I, DMF, and finally (vii) Dowex® 1x8 200 mesh ion-exchange column, H_2O. Yield: 44%.

4-(10-iododecyloxy)benzaldehyde (4). 1,10-Diiododecane (25 g, 63.4 mmol) was added to a mixture of 4-hydroxybenzaldehyde (1 g, 8.2 mmol) and potassium carbonate (2 g, 14.5 mmol) in dry *N,N*-dimethylformamide (25 mL). The reaction mixture was stirred at 80°C for 5 h, then cooled down to room temperature and diluted with CH_2Cl_2 (150 mL). The organic solution was washed with H_2O (3 x 100 mL), dried over anhydrous $MgSO_4$, filtered and the solvents were removed by rotary evaporation. The crude product was purified by flash chromatography on silica gel (2:1 CH_2Cl_2:petroleum ether), R_f 0.40, to give a colorless oil. Yield: 2.1 g (65%).

^{1}H NMR (400 MHz, $CDCl_3$) δ_H 9.86 (s, 1H), 7.82 (d, *J* = 8.8 Hz, 2H), 6.99 (d, *J* = 8.8 Hz, 2H), 4.02 (t, *J* = 6.3 Hz, 2H), 3.17 (t, *J* = 6.8 Hz, 2H), 1.80 (m, 4H), 1.36 (m, 12H); **^{13}C NMR** (100 MHz, $CDCl_3$) δ_C 190.88, 164.34, 132.07, 129.84, 114.84, 68.48, 33.60, 30.55, 29.49, 29.40, 29.35, 29.12, 28.58, 26.02, 7.41. **HRMS** (ESI-TOF) m/z 389.0984 ($C_{17}H_{25}O_2I$, $[M]^+$, requires 389.0978).

BODIPY 3. 4-(10-iododecyloxy)benzaldehyde (**4**) (2.1 g, 5.4 mmol) was dissolved in freshly distilled pyrrole (30 mL, 432 mmol) and the resulting solution was degassed by sparging with N_2 for 20 minutes before the addition of TFA (0.1 mL, 1.3 mmol). The mixture was stirred for 3 hours at room temperature, diluted with CH_2Cl_2 (100 mL) and then washed consecutively with H_2O (100 mL), $NaHCO_3$ (100 mL, 0.5M) and H_2O (100 mL). The organic extracts were dried over anhydrous $MgSO_4$, filtered and evaporated using a rotary evaporator. The excess pyrrole was removed using high vaccum to give the dipyrromethane as a dark viscous oil. The crude dipyrromethane was purified by flash chromatography on silica gel (2:1 CH_2Cl_2:petroleum ether), R_f 0.35, to give a green viscous oil. Yield: 2.5 g (94%). The dipyrromethane (2.5 g, 4.9 mmol) was dissolved in CH_2Cl_2 (200 mL) and DDQ (1.34 g, 5.9 mmol) was added. The reaction mixture was stirred at room temperature shielded from light for 1 hour. Then, Et_3N (6 mL, 43 mmol) was added, followed immediately by the addition of $BF_3{\cdot}(OEt_2)_2$ (5 mL, 40.5 mmol) and the reaction mixture was stirred at room temperature overnight. The organic solution was washed with H_2O (100 mL), NH_4Cl (100 mL, 0.5M), $NaHCO_3$ (100 mL, 0.5 M) and finally H_2O (100 mL), and then dried over anhydrous $MgSO_4$, filtered and evaporated to give a black viscous oil which was purified by column chromatography on silica gel (7:1 petroleum ether:ethyl acetate), R_f 0.20, to give **BODIPY 3** as a red-orange sticky solid. Yield: 717 mg (24%).

^{1}H NMR (400 MHz, $CDCl_3$) δ_H 7.91 (br s, 2H), 7.54 (d, *J* = 8.8 Hz, 2H), 7.04 (d, *J* = 8.8 Hz, 2H), 6.98 (d, *J* = 4.4 Hz, 2H), 6.55 (dd, *J* = 4.4, 1.9 Hz, 2H), 4.05 (t, *J* = 6.4 Hz, 2H), 3.19 (t, *J* = 7.3 Hz, 2H), 1.84 (m, 4H), 1.33 (m, 12H); **^{13}C NMR** (100 MHz, $CDCl_3$) δ_C 161.88, 147.68, 143.44, 134.95, 132.59, 131.48, 126.23, 118.36, 114.66, 68.45, 33.64, 30.60, 29.56, 29.46, 29.44, 29.28, 28.64, 26.14, 7.45; **^{19}F NMR** (377.5 MHz, $CDCl_3$) δ_F –143.19 (q, $J_{F\text{-}B}$ = 29.7 Hz); **HRMS** (ESI-TOF) m/z 531.1481 ($C_{25}H_{30}BN_2OF_2$, $[M\text{-}F^-]^+$, requires 531.1480)

Rotor 2. To a solution of **BODIPY 3** (240 mg, 0.43 mmol) in 16 mL of THF was added *N,N,N′,N′*-tetramethyl-1,3-propanediamine (3 mL, 17.9 mmol). The resulting mixture was stirred at room temperature overnight, during which time a dark-red waxy compound precipitated out from the reaction mixture. The solvent and excess of *N,N,N′,N′*-tetramethyl-1,3-propanediamine were removed by evaporation under reduced pressure and the crude product was washed several times with diethyl ether. This mono-charged intermediate, which

was used without further purification, was dissolved in DMSO (6 mL) and iodomethane (3 mL, 48.2 mmol) was added to the solution. After stirring the reaction mixture at room temperature overnight, the solvent was evaporated under reduced pressure to give a dark red crude product which was purified by column chromatography on silica gel (methanol, and then a mixture of 3:1 methanol:0.5 M NH_4Cl), R_f 0.2. Fractions were evaporated at 30°C to give a mixture of **rotor 2** and NH_4Cl which was further dissolved in methanol and successively filtered to remove most of NH_4Cl. The red-orange crude, which was still contaminated with NH_4Cl according to ^{1}H-NMR, was dissolved in methanol and a saturated solution of NH_4PF_6 in H_2O was added in order to exchange counter-ions. The precipitate was isolated by filtration, washed thoroughly with H_2O, methanol and diethyl ether. Finally, the red-orange solid was dissolved in acetone and passed through a Dowex® 1x8 200 mesh ion-exchange column (H_2O). Fractions were evaporated to dryness (at 30°C) to give **rotor 2** as a red-orange wax. Yield: 121 mg (44%).

^{1}H NMR (400 MHz, CD_3OD) δ_H 7.92 (br s, 2H), 7.60 (d, *J* = 8.3 Hz, 2H), 7.13 (d, *J* = 8.3 Hz, 2H), 7.05 (d, *J* = 3.4 Hz, 2H), 6.63 (dd, *J* = 3.4, 1.4 Hz, 2H), 4.10 (t, *J* = 6.3 Hz, 2H), 3.42 (m, 6H), 3.23 (s, 9H), 3.17 (s, 6H), 2.35 (m, 2H), 1.83 (m, 4H), 1.42 (m, 12H); **^{13}C NMR** (100 MHz, CD_3OD) δ_C 163.44, 149.01, 144.52, 136.01, 133.79, 132.58, 127.20, 119.50, 115.77, 69.40, 66.47, 63.92, 61.61, 54.07, 51.41, 30.58, 30.52, 30.44, 30.27, 27.42, 27.13, 23.67, 18.68; **^{19}F NMR** (377.5 MHz, CD_3OD) δ_F –145.68 (q, $J_{F\text{-}B}$=28.6 Hz); **HRMS** (ESI-TOF) m/2z 284.2023 ($C_{33}H_{51}BN_4OF_2$, $[M\text{-}2Cl^-]^+$, requires 284.2057)

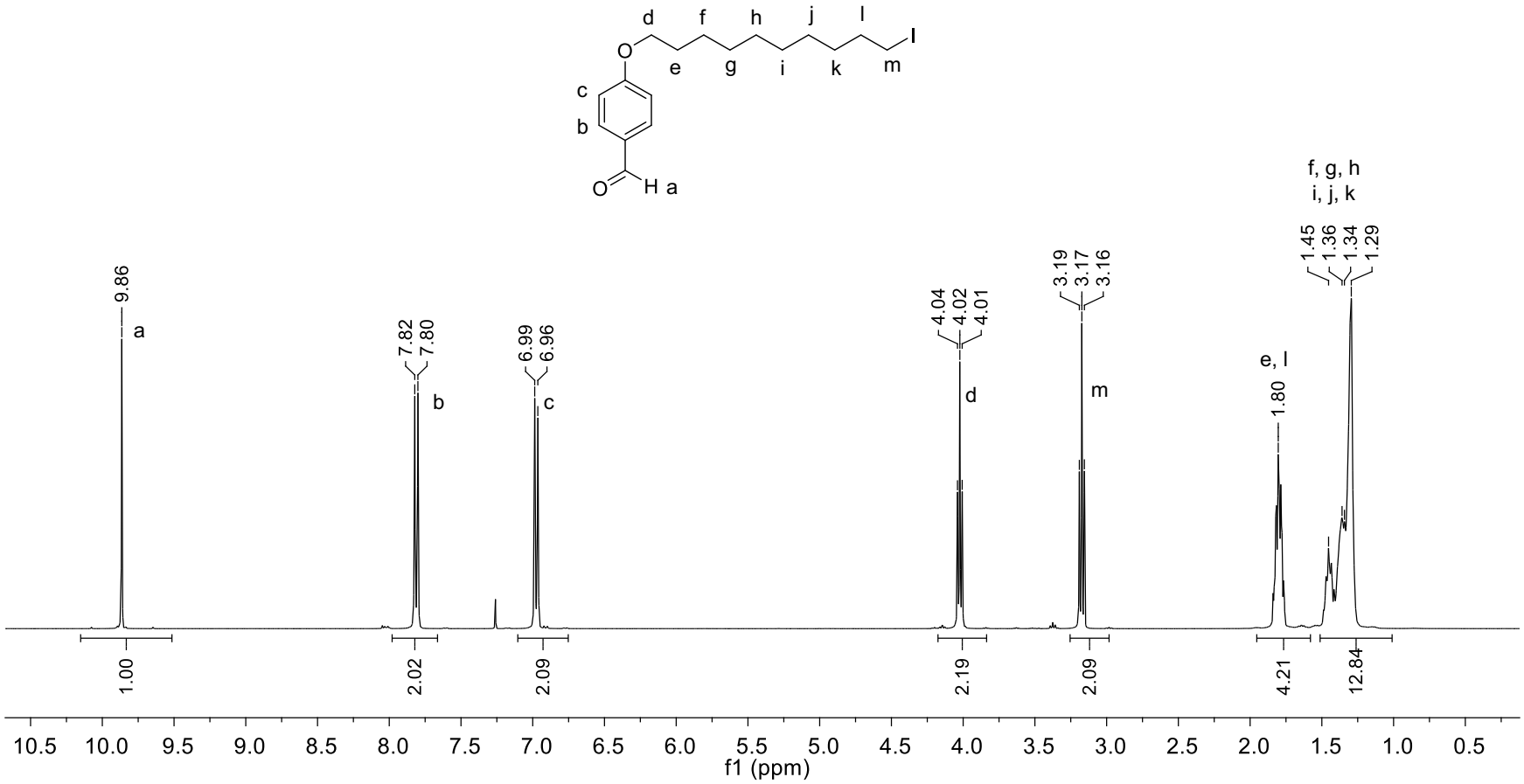

Figure S7. ^{1}H NMR spectrum of **4** (400 MHz, $CDCl_3$).

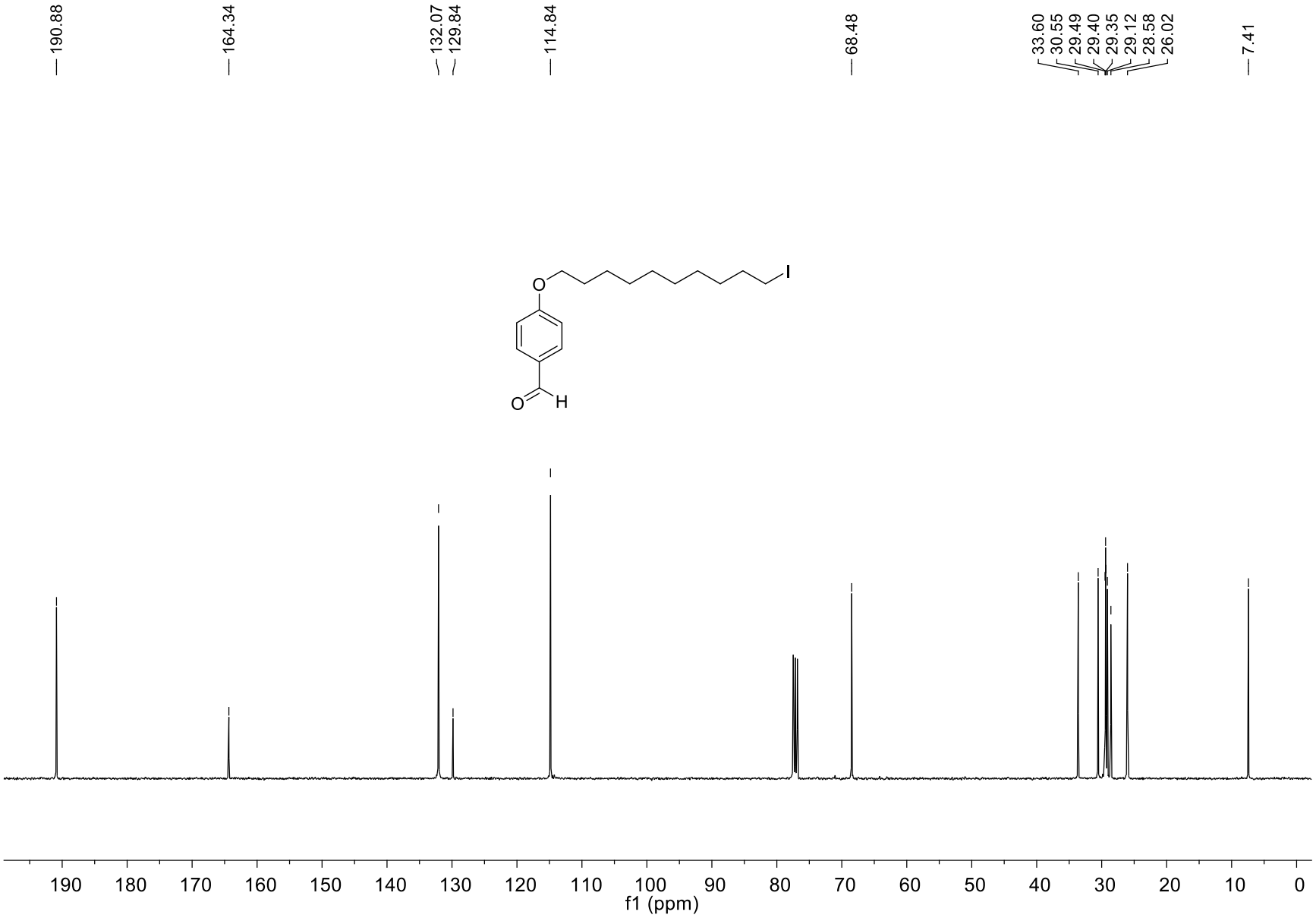

Figure S8. ^{13}C NMR spectrum of **4** (100 MHz, $CDCl_3$).

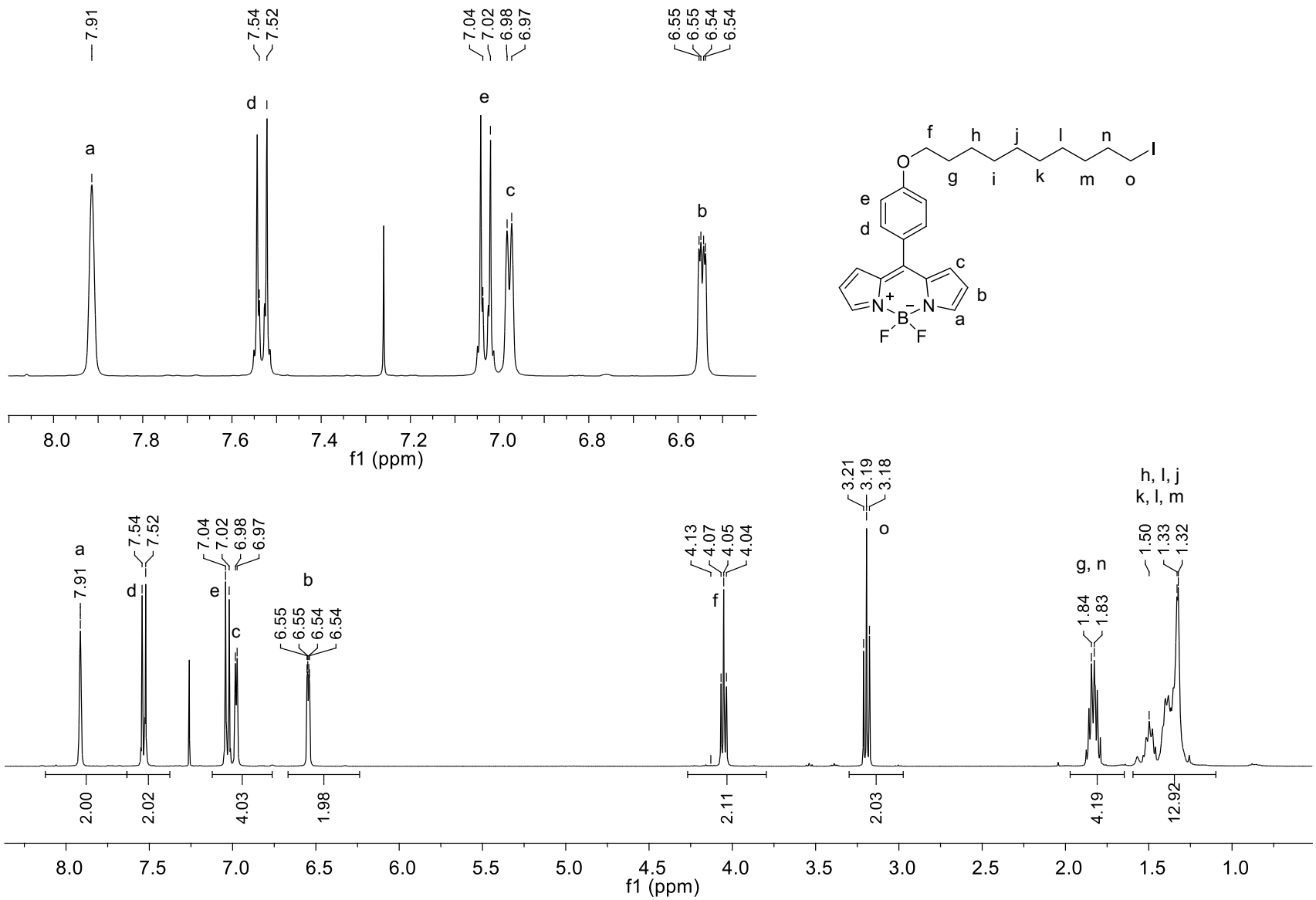

Figure S9. ^{1}H NMR spectrum of **BODIPY 3** (400 MHz, $CDCl_3$).

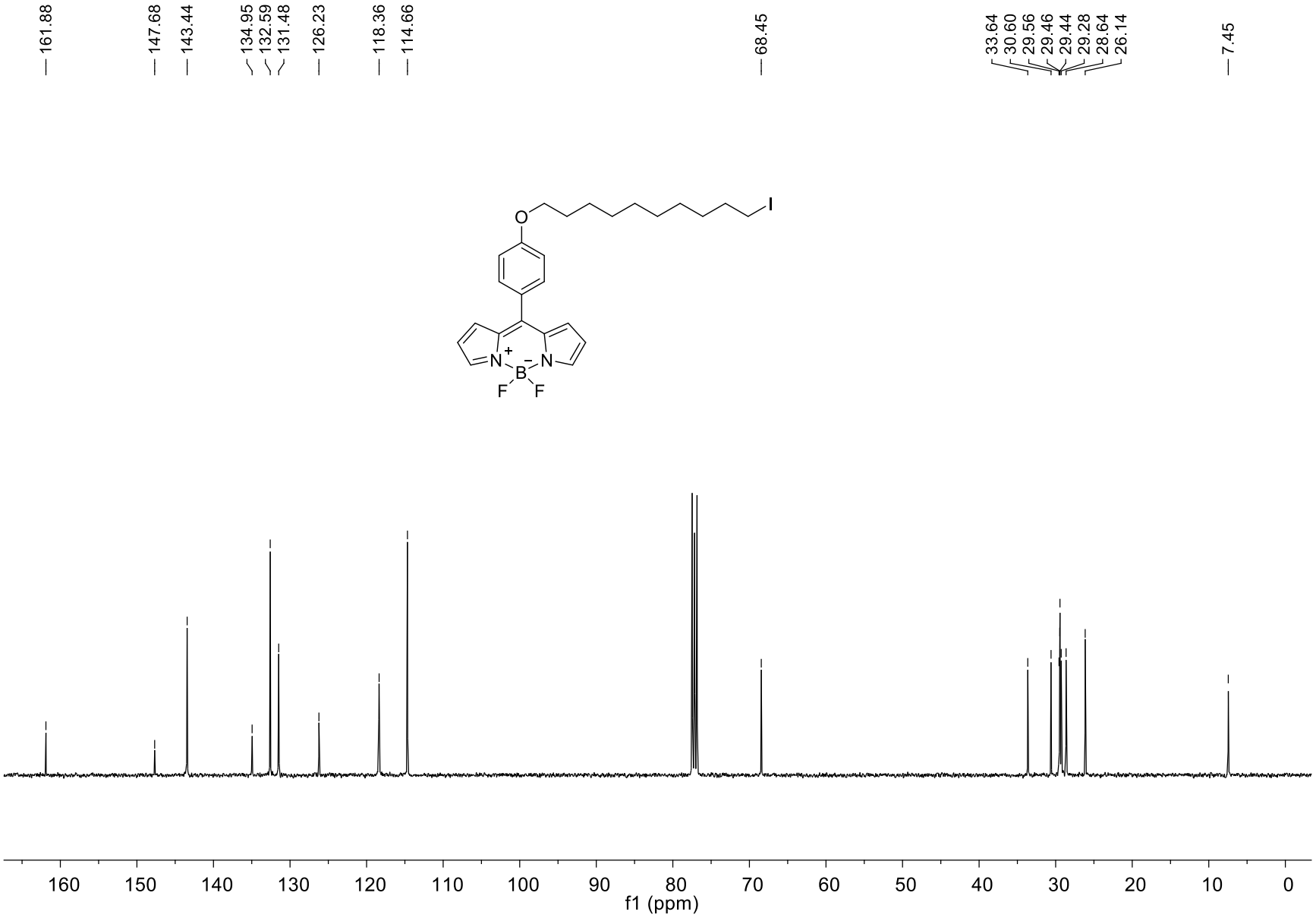

Figure S10. ^{13}C NMR spectrum of **BODIPY 3** (100 MHz, $CDCl_3$).

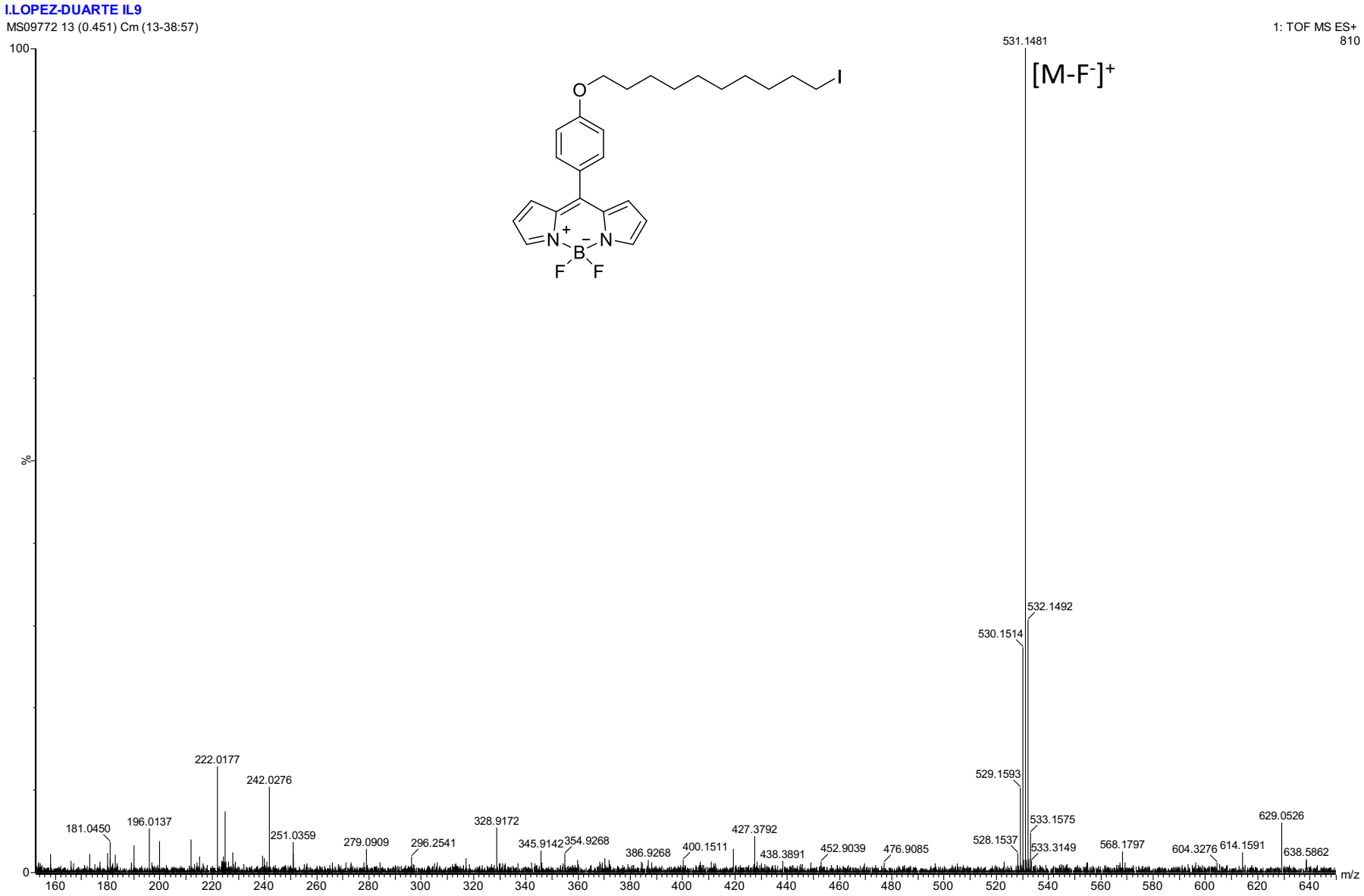

Figure S11. HRMS (ESI-TOF) mass spectrum of **BODIPY 3**.

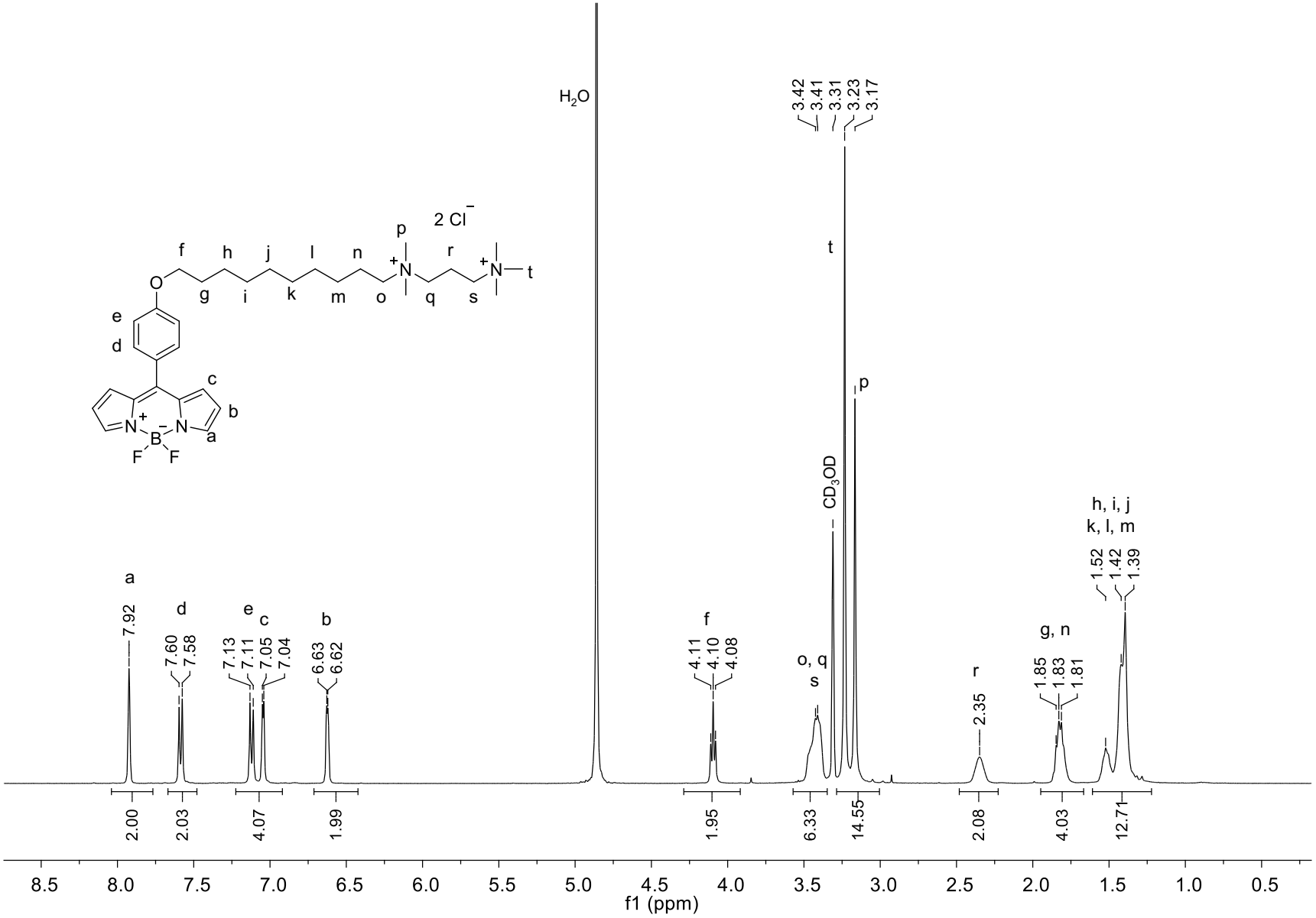

Figure S12. ^{1}H NMR spectrum of **rotor 2** (400 MHz, CD_3OD).

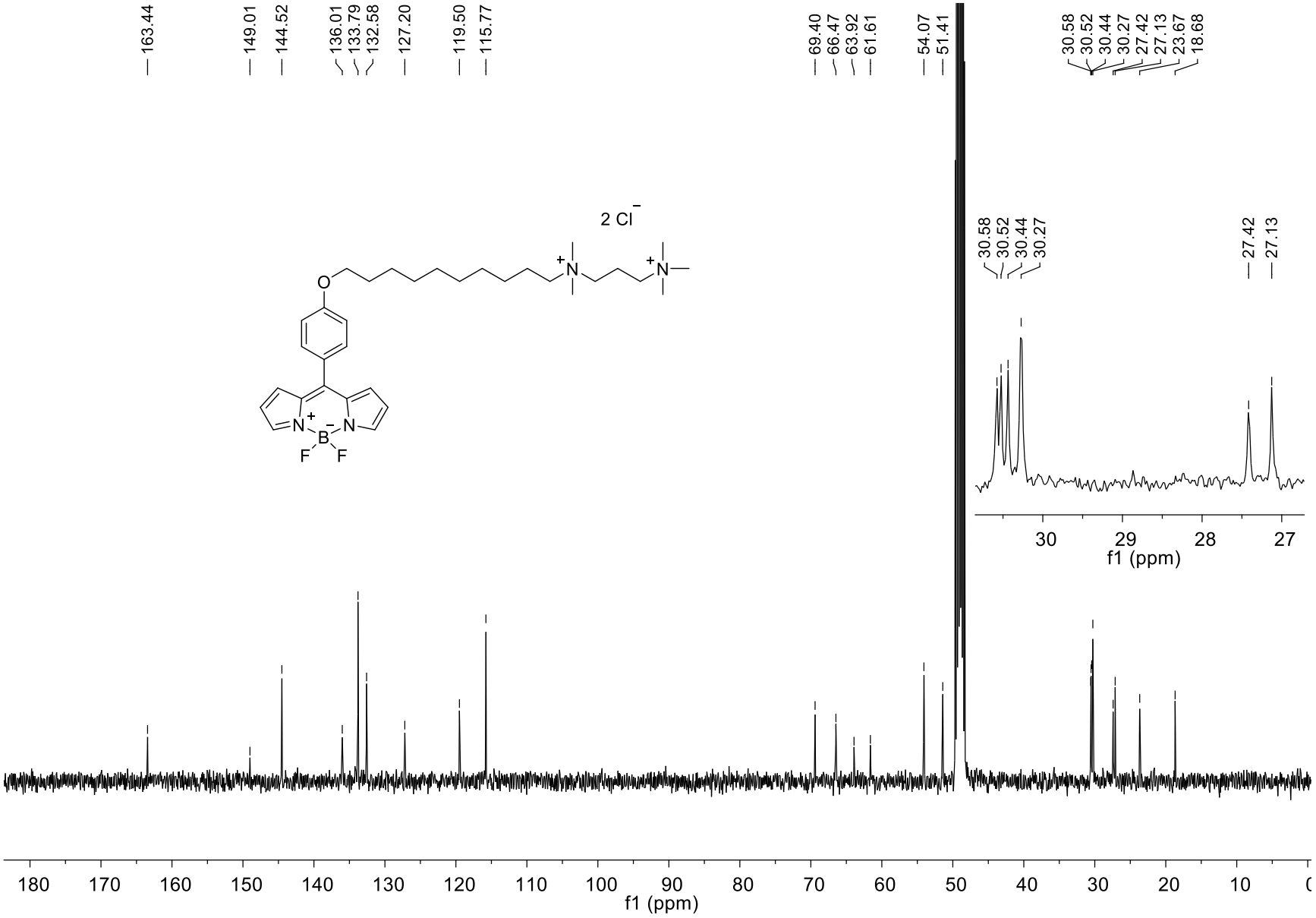

Figure S13. ^{13}C NMR spectrum of **rotor 2** (100 MHz, CD_3OD).

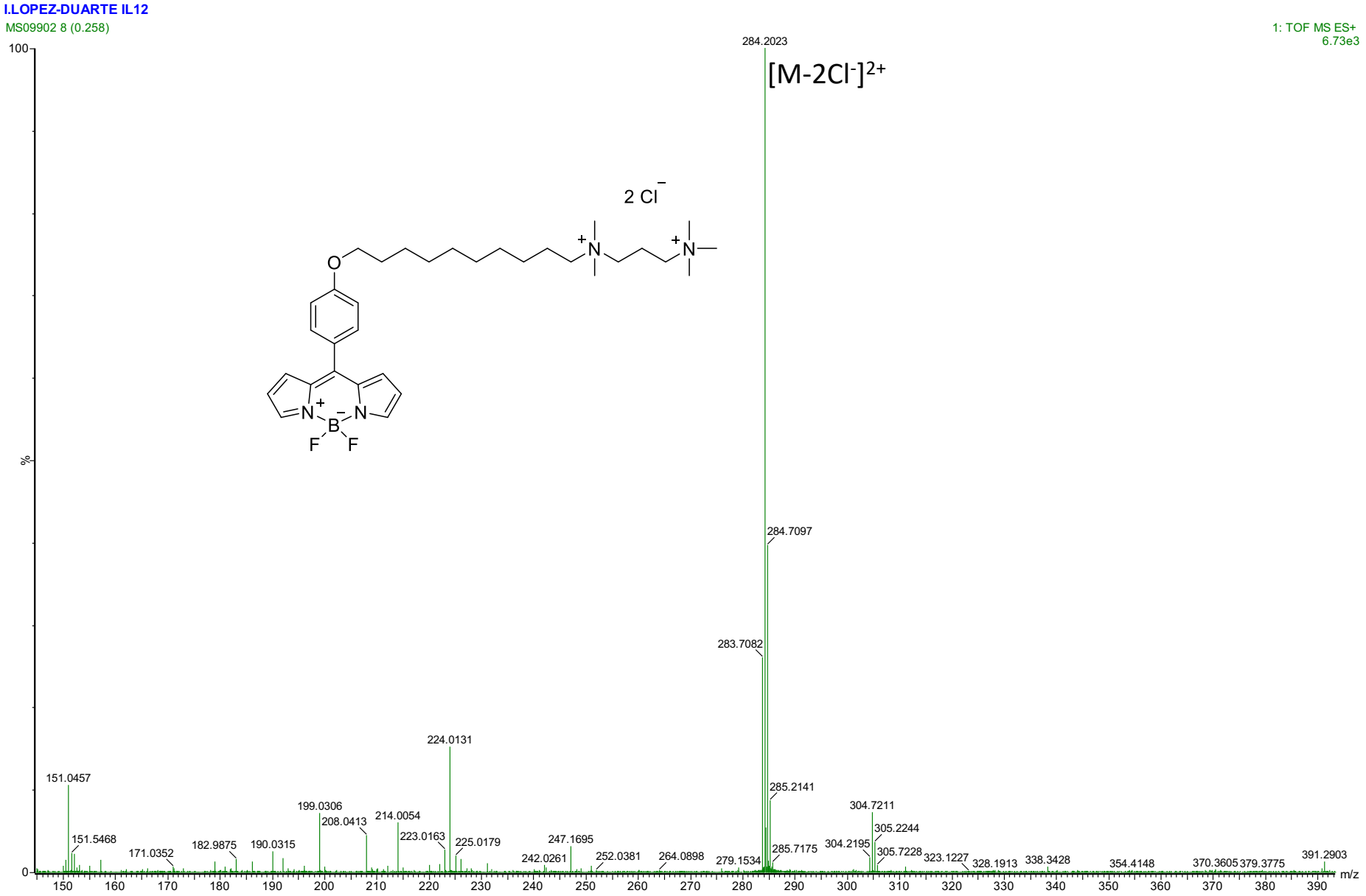

Figure S14. HRMS (ESI-TOF) mass spectrum of **rotor 2**.

3. Supplementary References

1. (a) Wagner, R. W.; Lindsey J. S. *Pure & Appl. Chem*. **1996**, *68 (7)*, 1373-1380. (b) Loudet, A.; Burgess, K. *Chem. Rev*., **2007**, *107*, 4891-4932.